Research article

JGS
Journal of the Geological Society

Published online July 22, 2020

https://doi.org/10.1144/jgs2020-074 | Vol. 177 | 2020 | pp. 1168–1185

Nature and significance of rift-related, near-surface fissure-fill networks in fractured carbonates below regional unconformities

Kit Hardman[1,2], Robert E. Holdsworth[1,3]*, Edward Dempsey[2] and Ken McCaffrey[1,3]

[1] Department of Earth Sciences, Durham University, Durham DH1 3LE, UK
[2] Department of Geography, Environment and Earth Sciences, University of Hull, Hull HU6 7RX, UK
[3] Geospatial Research Ltd, Durham DH1 4EL, UK
REH, 0000-0002-3467-835X; ED, 0000-0002-8425-2226
* Correspondence: r.e.holdsworth@durham.ac.uk

Abstract: Fissure-fill networks are a widely recognized, but relatively little described, near-surface phenomenon (<1–2 km) hosted in carbonate and crystalline basement rocks below regional unconformities. Faults and fractures in otherwise tight Devonian carbonate basement rocks of the Tor Bay region, Devon, SW England are associated with the development of millimetre- to decametre-wide fissures containing red-coloured early Permian sedimentary material, vuggy calcite mineralization and wall rock collapse breccia. These features preserve evidence about the style and history of fault deformation and reactivation in near-surface settings and on fluid-related processes, such as elutriation and/or mineralization. Field observations, palaeostress analysis and fracture topology analyses show that the rift-related faults and fractures created a network of long-lived open cavities during the development of the Portland–Wight Basin in the early Permian. Once formed, they were subjected to episodic, probably seismically induced, fluid fluxing events and local karstification. The large, well-connected networks of naturally propped fractures were (and possibly still are) important fluid migration pathways within otherwise low-permeability host rocks. These structures are probably equivalent to those observed in many other rift-related, near-surface tectonic settings and suggest that the Tor Bay outcrops can be used as a global analogue for sub-unconformity open fissure systems hosted in low-permeability basement rocks.

Supplementary material: Appendix A is available at https://doi.org/10.6084/m9.figshare.c.5023103

Received 23 April 2020; **revised** 2 June 2020; **accepted** 15 June 2020

Cavern systems are widely developed across a range of scales in carbonate sequences worldwide and are known to be sustained as open features to depths >2 km due to the cohesion and relatively high tensile strength of most lithified limestones (e.g. Smart *et al.* 1988; van Gent *et al.* 2010). Many modern examples are associated with younger sedimentary fills and low-temperature carbonate mineralization. These features are known to strongly control present day fluid flow pathways and processes and, more generally, the hydraulic behaviour of carbonates in the near subsurface (e.g. Popov *et al.* 2009).

Ancient and modern carbonate cavity systems are commonly referred to as karst features and their formation mechanisms are typically attributed substantially to dissolution processes. However, very similar features are also recognized in other strong host rocks fractured in near-surface environments (<1–2 km depth), such as basalts (e.g. Angelier and Mechler 1977; Schlische and Ackermann 1995; Walker *et al.* 2011) and crystalline basement rocks (e.g. Beacom *et al.* 1999; Siddoway and Gehrels 2014; Holdsworth *et al.* 2019). Solution processes are relatively minor or absent in most of these cases. Theoretical considerations and analogue modelling studies show that the relatively high strength of carbonate and crystalline rocks will tend to favour the formation of subvertical dilational fissures in the near-surface during episodes of rift-related normal or strike-slip faulting (Fig. 1a–c; e.g. Sibson 1996; Ferrill and Morris 2003; van Gent *et al.* 2010; von Hagke *et al.* 2019). We should therefore expect such features to be widely preserved in ancient settings where fractured carbonates (or crystalline basement rocks) form a basement that was exposed at the palaeosurface below regional erosional unconformities during the early stages of rifting prior to burial. Given the frequent global development of hydrocarbon and geothermal reservoirs in fractured carbonates located close to regional erosional unconformities in the subsurface (Yang *et al.* 2014; Narayan *et al.* 2018), these fault-related fissure systems are likely to be of potential economic significance.

Massively dilated, ancient examples of carbonate-hosted fault zones are already known – for example, the folded Tertiary carbonates in the UAE and Oman (van Gent *et al.* 2010), where they are filled with carbonate veins, fractured wall rocks and laminated sediment fills. Similar normal fault fissure fills – thought to be Triassic to early Jurassic in age based on fossil evidence – are widely recognized in the fractured Carboniferous limestone basement that underlies the regional post-Variscan unconformity in the Bristol Channel Basin (e.g. Wall and Jenkyns 2004; Wright *et al.* 2009; Woodcock *et al.* 2014, their fig. 13).

We describe here in detail the nature and significance of fissure systems filled with sedimentary material, breccia and calcite-dominated mineral deposits hosted in fractured Devonian limestones cropping out on the western onshore flanks of the offshore Portland–Wight Basin in Tor Bay, SW England (Fig. 2). We examine the diverse architecture of these fissure fills and their associations with rift-related normal faults, the nature and mechanisms of filling and discuss the significance of our findings for fluid flow and fluid reservoir development in the subsurface.

Geological setting

Regional context and stratigraphy

Tor Bay in SW England lies within the English Riviera UNESCO Global Geopark, stretching 9 km from Hope's Nose [SX 94741 63546] southwards to Berry Head [SX 94563 56538] (Fig. 2). A structurally complex basement sequence of Devonian limestones

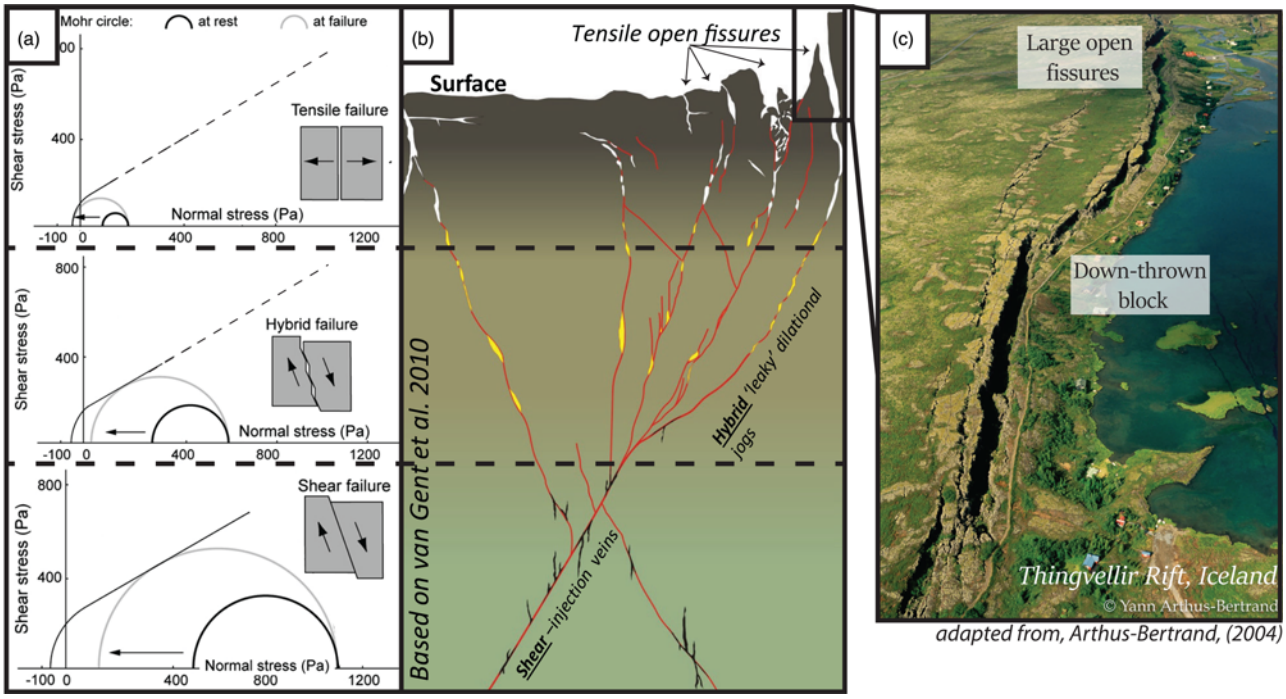

Fig. 1. (a) Hypothetical Mohr circles illustrating the translation from tensile failure at the surface to normal faulting (shear fracture) at depth (after van Gent *et al.* 2010). (b) Cross-section view of fractures generated in an analogue model (van Gent *et al.* 2010) illustrating fault cavity architectures for different depth zones. (c) Aerial photograph of Thingvellir Rift, Iceland showing large tensile fissures developed in basalts at the surface related to the development of a normal fault at depth. Photograph used with permission from Yann Arthus-Bertrand, part of the *Earth from Above* collection (www.yannarthusbertrand2.org; Arthus-Bertrand 2004, 2020).

and calcareous mudstones was deformed during the Variscan Orogeny (Coward and McClay 1983). It includes, from oldest to youngest: the Early Devonian Meadfoot Group; the Mid Devonian Nordon Formation; the Brixham (or Torbay) Limestone Formation; and the Late Devonian Saltern Cove Formation (Strange 2001). Devonian basaltic tuffs and intrusive dolerites occur at Saltern Cove, Black Head and Oddicombe Beach (Fig. 2) (Ussher 1903).

A little deformed and shallowly dipping (<10°) cover sequence of red, early Permian sandstones and breccias outcrops mainly within the central part of the Tor Bay coast (Fig. 2) (George Anniss and Smith 1927; Shannon 1928; Strange 2001). These rocks belong to the Torbay Breccia Formation, part of the Exeter Group (Ussher 1903; Henson 1971). They form a well-bedded sedimentary succession, starting with alluvial conglomerates and depositional breccias at the base, before sharply transitioning to younger cross-bedded and well-sorted aeolian sandstones. The basement and cover are separated by a regional-scale, post-Variscan erosive angular unconformity known locally as the Goodrington Unconformity, best exposed at [SX 89539 58742].

Extensive outcrops of Permo-Triassic and Jurassic sandstones occur along the South Devon–Dorset coastline to the east of Tor Bay, which also form key potential reservoir rocks in the offshore Southwest Approaches petroleum system (Shail and Leveridge 2009 and references cited therein). Although separated by the NW–SE-trending Stickleback–Lustleigh fault zone, the Tor Bay area lies on the western flanks of the offshore Portland–Wight Basin (Fig. 2; Harvey *et al.* 1994; Underhill and Stoneley 1998). The form of the Tor Bay coastline and the margins of the offshore basin are significantly controlled by regional-scale, subvertical fault zones.

Pleistocene karst systems are widely developed in the Devonian limestones onshore (e.g. Kent's Cavern; Ussher 1903; Lundberg and McFarlane 2007), together with interglacial raised beach sediments (Strange 2001; Leveridge and Hartley 2003).

Structural evolution

During the Variscan Orogeny, northwards-directed contractional deformation led to the development of northwards-verging minor folds, cleavages and thrust faults in the Devonian basement sequences (e.g. Coward and McClay 1983). Following uplift, exhumation and regional erosion, the exposed limestone basement around Tor Bay experienced one or more phases of extensional tectonics, subsidence and sedimentation, leading to the formation of large, steeply dipping to subvertical NNE–SSW and east–west to ENE–WSW faults and the regional-scale Goodrington Unconformity (Harvey *et al.* 1994; Shail and Wilkinson 1994) (Fig. 2). Permian extension here is thought to be related to the post-orogenic collapse of the uplifted Variscan orogenic belt (Harvey *et al.* 1994; Ruffell and Shelton 2000). Some large basin-bounding faults are seen onshore (e.g. at Crystal and Saltern coves), while others are inferred to lie just offshore, with smaller fracture arrays occurring in aligned swarms and corridors throughout Tor Bay (Fig. 2). The open fissures associated with both fracture sets are known to be filled with zoned calcites, complex breccias and significant volumes of red sedimentary material (e.g. Richter 1966).

Following a period of tectonic quiescence in the Triassic, active rifting resumed during the Jurassic. This extension was centred offshore to the east of Tor Bay, generating large sedimentary depocentres off the Dorset coast in the Portland–Wight Basin (Underhill and Stoneley 1998). Unequivocal evidence for this phase of extension is not observed within the study area because there are no exposed Jurassic rocks onshore, but it is clearly seen offshore in seismic reflection profiles (e.g. Underhill and Stoneley 1998).

A later Cenozoic disconformity occurs in the Eocene–Oligocene strata of southern Britain and reflects a further period of regional uplift. At around this time, several kilometres of sinistral strike-slip motion are thought to have occurred along the regional NW–SE Sticklepath–Lustleigh Fault Zone (Fig. 2; Holloway and Chadwick 1986). This NW–SE fault zone presently separates the onshore Tor

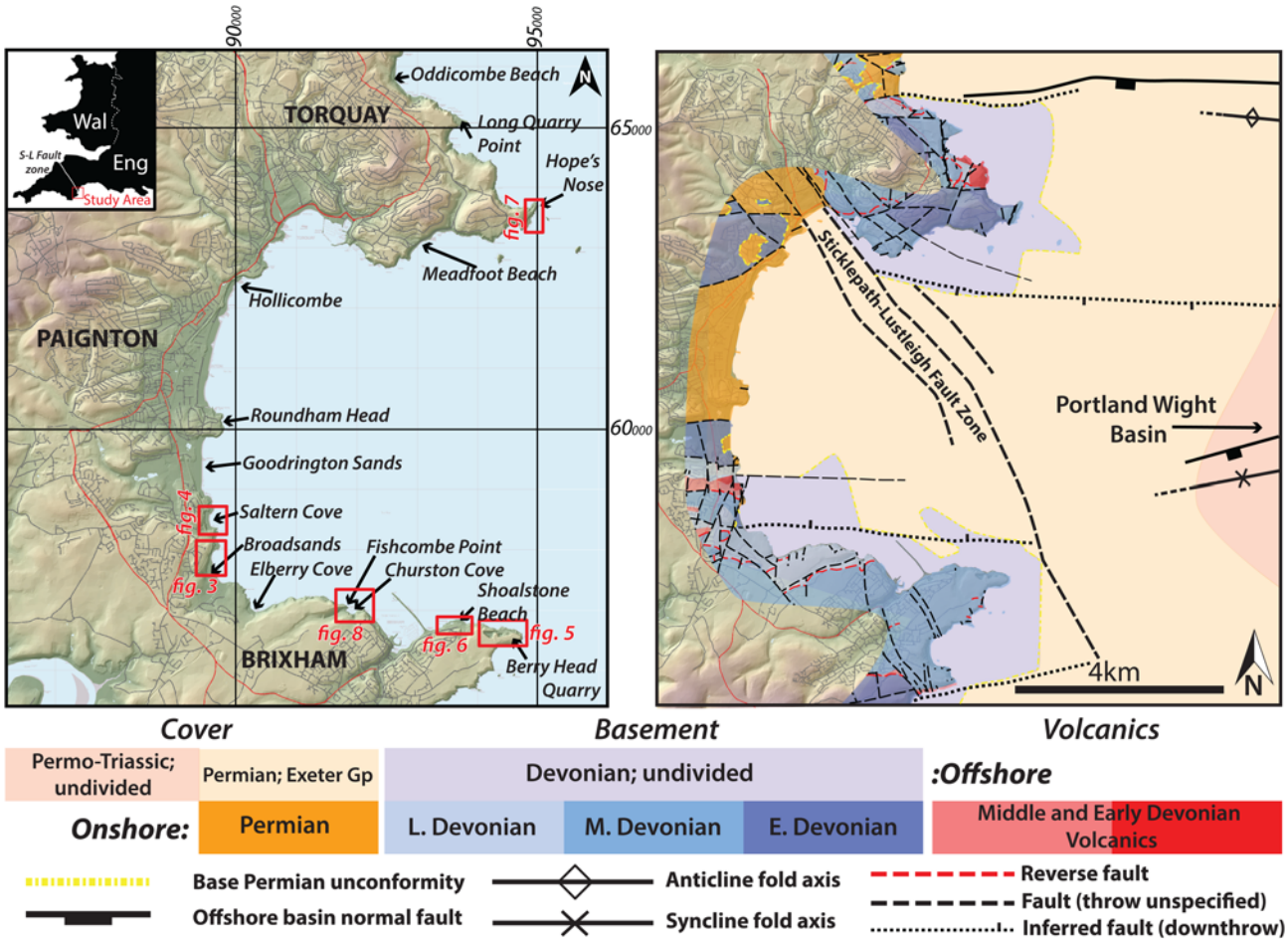

Fig. 2. Left-hand panel: simplified location map of Tor Bay with the key locations and study areas shown by red boxes. Right-hand panel: simplified coastal onshore–offshore geological map of the main lithological and stratigraphic units and structures in Tor Bay. Adapted from British Geological Survey (2004), Harvey *et al.* (1994) and data provided with permission by EDINA Digimap (OS VectorMap® Local [TIFF geospatial data], OS Terrain 5 [ASC & SHAPE geospatial data] scale 1:10000, tiles sx85ne, sx85se, sx86ne, sx86se, sx95ne, sx95nw, sx95sw, sx96ne, sx96nw, sx96se, sx96sw, updated 27 June 2018, Ordnance Survey (GB), using EDINA Digimap Ordnance Survey Service, https://digimap.edina.ac.uk) (DiGRock250k [SHAPE geospatial data], scale 1:250000, tiles GB, updated 31 December 2013, BGS, using: EDINA Geology Digimap Service, https://digimap.edina.ac.uk) (DiGMapGB-50 [SHAPE geospatial data], scale 1:50000, tiles ew339,ew350, updated 30 November 2016, BGS, using EDINA Geology Digimap Service, https://digimap.edina.ac.uk).

Bay area from the offshore Portland–Wight Basin located further to the east (Fig. 2).

Field and laboratory methods

Fracture systems and their fills were studied at 14 localities around Tor Bay (Fig. 2), where they are well exposed in the Devonian carbonate basement located close to the Goodrington Unconformity in coastal cliffs, wave-cut platforms and quarries (Fig. 2). Structural geometries were recorded through the collection of orientation data, with brittle fault kinematics measured from the offsets of markers in the host rocks, the local preservation of slickenline lineations and the preservation of asymmetrical shear criteria, such as en echelon veins and slickenline steps (Petit 1987). The relative ages of fractures and their associated fills were ascertained in the field from observations of cross-cutting relationships. In exceptionally well-exposed cliff sections and rock platforms, observations and interpretations were also made using low-level areal images collected by a drone. Representative samples of oriented hand specimens were collected from mineral and sediment fills of fractures and were used to study the microstructure and relative age relationships of mineralization and cementation using transmitted light optical microscopy.

As many of the fracture systems studied included faults with slickenline lineations, we used palaeostress inversion techniques to determine an approximation of the stress conditions responsible for their formation. This was carried out using WinTensor software (Delvaux and Sperner 2003), which uses both the PBT axes method and the improved right dihedron method of Angelier and Mechler (1977) and Delvaux *et al.* (1995). These techniques have a consistent assumption that the slip vector data recorded in the field are parallel to the ideal shear component of the resolved stress tensor (Wallace 1951; Bott 1959). They are most appropriate where the host rock is mechanically isotropic, fault displacements are small and where data are measured across a broad range of fault plane orientations (Angelier 1991).

To quantify the fracture connectivity and volume of sediment fills in the Devonian basement, a drone-based orthorectified virtual outcrop model was created for one very well-exposed rock platform at Shoalstone Beach (Fig. 2) with an effective viewing resolution of 1–2 cm. This was then interpreted manually and ground-truthed during subsequent fieldwork to generate a fracture trace map. This map was used to quantify fracture attributes, both manually and using the FracPaQ MatLab extension (Healy *et al.* 2017). The relative connectivity of the fracture network was determined using fracture topology (for details, see Sanderson and Nixon 2015), a characterization technique that simplifies a 2D fault or fracture network into discrete branches and nodes. The ratios between different types of nodes (I–Y or Y–X) and branches can be used to

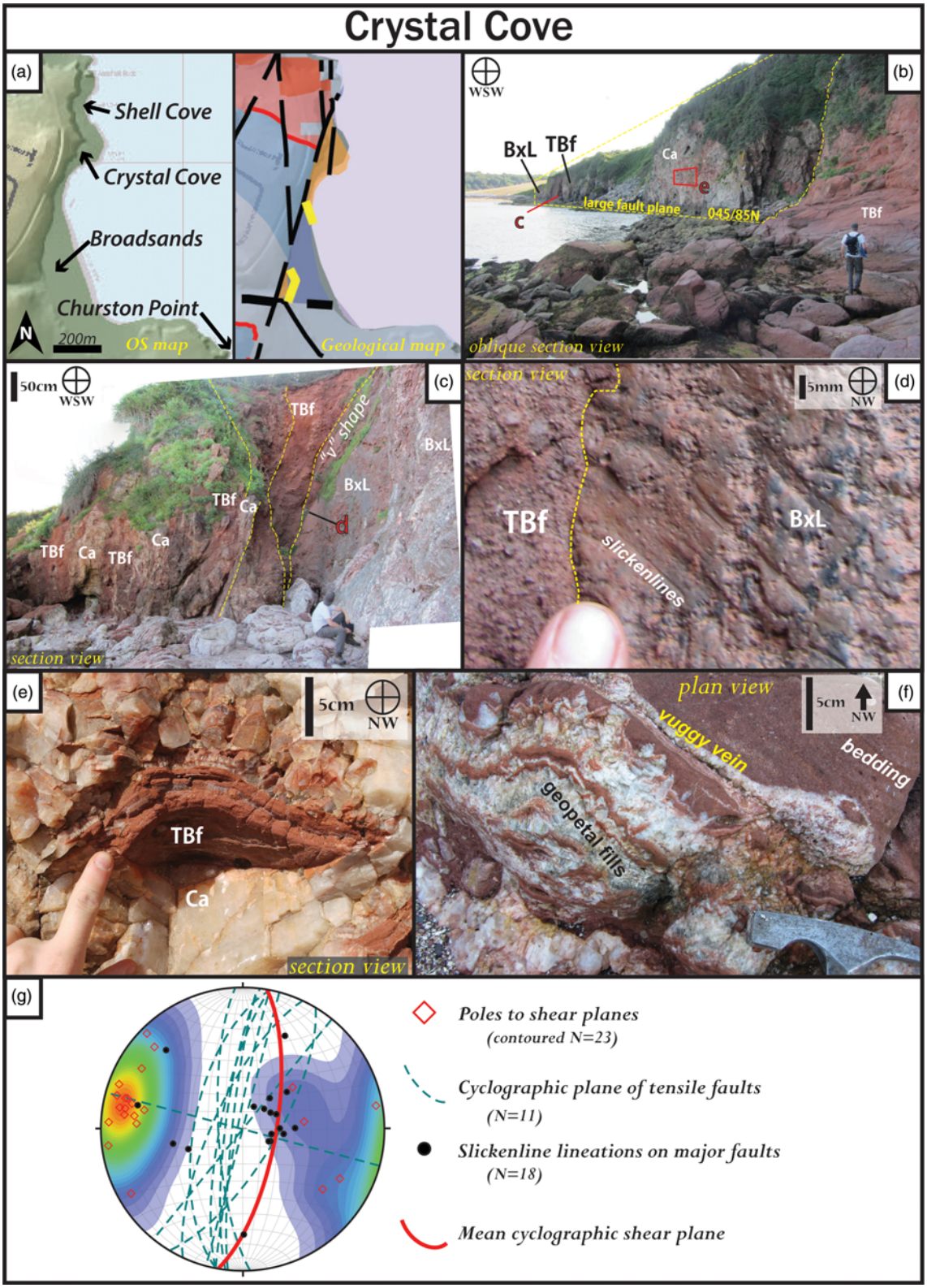

Fig. 3. Field photographs and location map of large faults at Crystal Cove (for location, see Fig. 2). (**a**) Maps showing key location names (left) and basic geology (right); for key, see Figure 2. (**b**) View of large fault surface separating Brixham Limestone Formation (BxL) and Torbay Breccia Formation (TBf) with a 'wall' of geopetal clastic sediment infill and calcite mineralization (Ca). Locations of Figure 3c, e are also shown [SX 89702 58039]. (**c**) Cross-section view of the large fault in part (b) showing a *c.* 40 m wide V-shaped fault aperture filled with red sandstone–breccia and complex calcite mineralization [SX 89541 57918]. (**d**) Slickenlines seen on the fault wall at the contact between the fault sediment infill and the limestone host rock along the major fault in part (c) [SX 89541 57918]. (**e**) Geopetal sediment accumulation in a conical shaped pile within a calcite mineralized fault plane, location shown in part (b) [SX 89590 57996]. (**f**) Plan view of fault cavity infill with successive syntaxial calcite mineralization and sediment infilling giving a strata-like banded appearance reflective of repeated opening history [SX 89619 58614]. (**g**) Stereographic projection of contoured poles to shear fracture planes, mean cyclographic shear plane, slickenline lineations and tensile fracture planes.

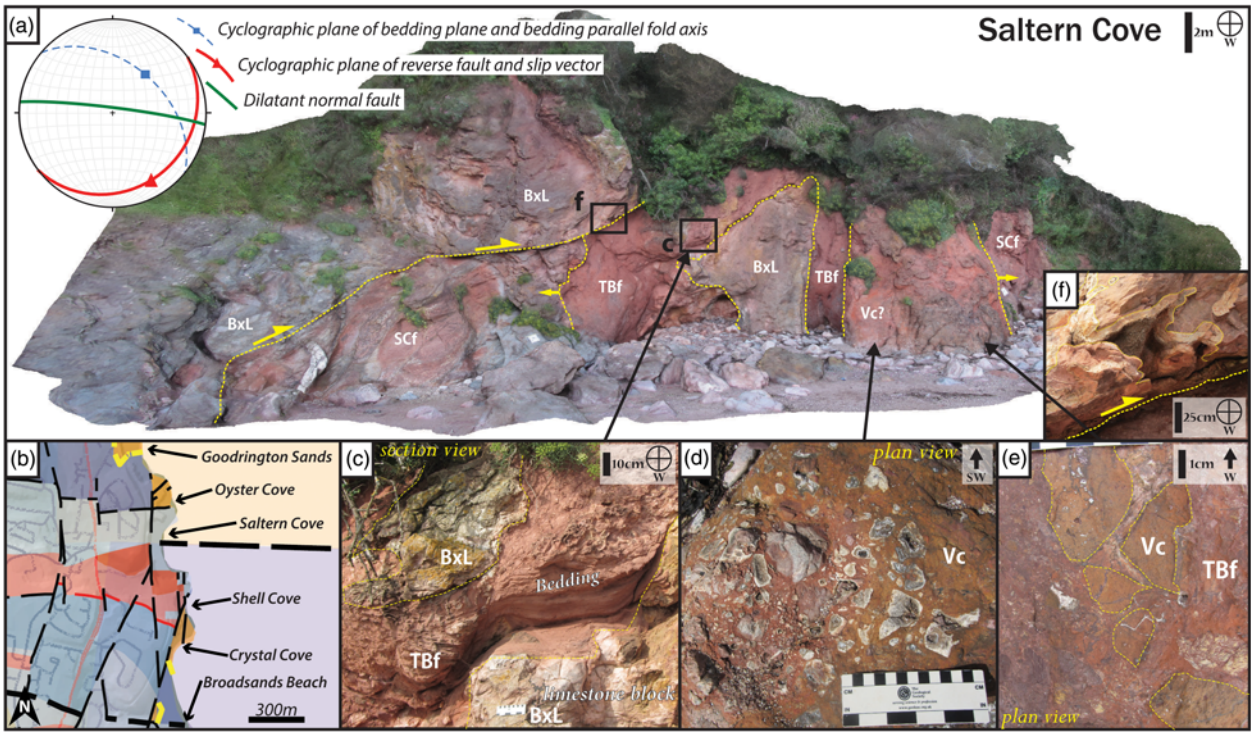

Fig. 4. Virtual outcrop model and field photographs from Saltern Cove (for location, see Fig. 2). Model and photographs show faulted Brixham Limestone Formation (BxL) and Saltern Cove Formation mudstones (SCf), infilled by Volcaniclastic material (Vc) and bedded sediment of the Torbay Breccia Formation (TBf). (**a**) Annotated 3D virtual outcrop model. Inset shows the stereographic projection of data from the reverse/thrust fault and slickenlines, the dilatant fault and the bedding of the overlying limestone and a bedding-parallel fold axis [SX 89488 58535]. (**b**) Local geological map with main outcrops labelled; for key, see Figure 2. (**c**) Section view of bedded sediment overlying the fallen limestone block. Location shown in part (a). (**d**) Zoned volcaniclastic tephra within the tensile normal fault; orange material is fine-grained tuff, with suspended volcanic clasts. (**e**) Breccia material infilling the normal tensile fault with clasts of brecciated orange volcaniclastic material set in a red sandstone matrix. (**f**) Cross-section view of limestone-hosted vuggy calcite-lined cavities in the hanging wall of the thrust fault.

determine the relative connectivity and spatial characteristics of the network. In addition, areal and volumetric calculations of the amounts of fracture fill were undertaken using the Image Processing toolbox of MatLab (see Supplementary Material).

Post-Variscan fracture architectures and geological associations

Brittle fractures are well-preserved, cross-cutting Devonian basement rocks and the lowermost parts (<5 m above basement) of Permian cover sequences around Tor Bay. These structures are characteristically highly dilational in character and consist of three distinct void-like forms described in the following sections.

Subvertical forms

Steeply dipping to subvertical structures are the dominant form around Tor Bay. Two categories occur: large normal faults with apertures of up to 40 m; and 10–100 m wide fracture corridors made up of fractures that individually have apertures of <1 m. Note that, throughout this paper, we use the term aperture to refer to the width of a fracture, including any fill – that is, the kinematic aperture of Ortega *et al.* (2006). Large normal faults at Crystal Cove [SX 89656 58057], a 400 m coastal section on the north side of Broadsands Beach, exposes a linked array of three major, subvertical NNE–SSW faults with apertures up to 40 m wide (Fig. 3a–c). Red clastic sedimentary material intercalated with extensive vuggy calcite mineralization fills the fault fissures (Fig. 3c, e, f). A series of discrete slip surfaces with calcite slickenfibres (e.g. Fig. 3d) are recognized separating panels of sediment infill, brecciated basement wall rocks and dilatant calcite mineral fills (Fig. 3b–f). The slickenfibres display normal dextral shear senses, with rakes varying from 63° to 90°, along planes that strike from 003° to 043° and dip from 68° to 86° E (Fig. 3g). These sediment fills are distinctly zoned, with each widening (increasing in aperture) towards the overlying palaeosurface unconformity in a V-shape (e.g. Fig. 3c). These features probably formed as filled fissure cavities, each zone representing an individual dilatant opening event of the fissure. The cavity widens with each movement, creating new spaces that were infilled by sediment and/or by minerals precipitated from circulating hydrothermal or meteoric fluids. The repeated overprinting of slickenfibres and zoned fills suggests multiple reactivation events, with synchronous shear and tensile fracturing behaviour close to the palaeosurface represented by the immediately adjacent base-Permian unconformity.

About 200 m north of Crystal Cove, a small inlet called Shell Cove (Fig. 3a) [SX 89643 58217] preserves the unconformable contact between the Devonian limestone basement and the Permian clast-supported breccia and interbedded sandstone cover. The lowermost layers of this cover sequence are interpreted as flash-flood deposits and contain clasts of the underlying limestone basement (Thomas 1909; Henson 1971). Subvertical NNE–SSW-trending sandstone and breccia-filled fractures are seen to cut both the limestone basement and the lowest 2–3 m of the overlying breccia. These rocks are then disconformably overlain by cross-bedded, finely laminated sandstone. It is difficult to demonstrate conclusively that the sedimentary material filling the fracture cavity is continuous with these Permian sandstones, but the lithologies are identical in composition, grain size and rounding. We therefore suggest that the cross-bedded sandstone either forms the sediment source or immediately post-dates the sediment fills in the underlying fractures and that both were deposited under similar environmental conditions.

East–west major faults are best observed at Oddicombe Beach [SX 92645 66127] and Saltern Cove [SX 89543 58377] (Figs 2 and 4). In the latter locality, a large east–west-trending fault system is

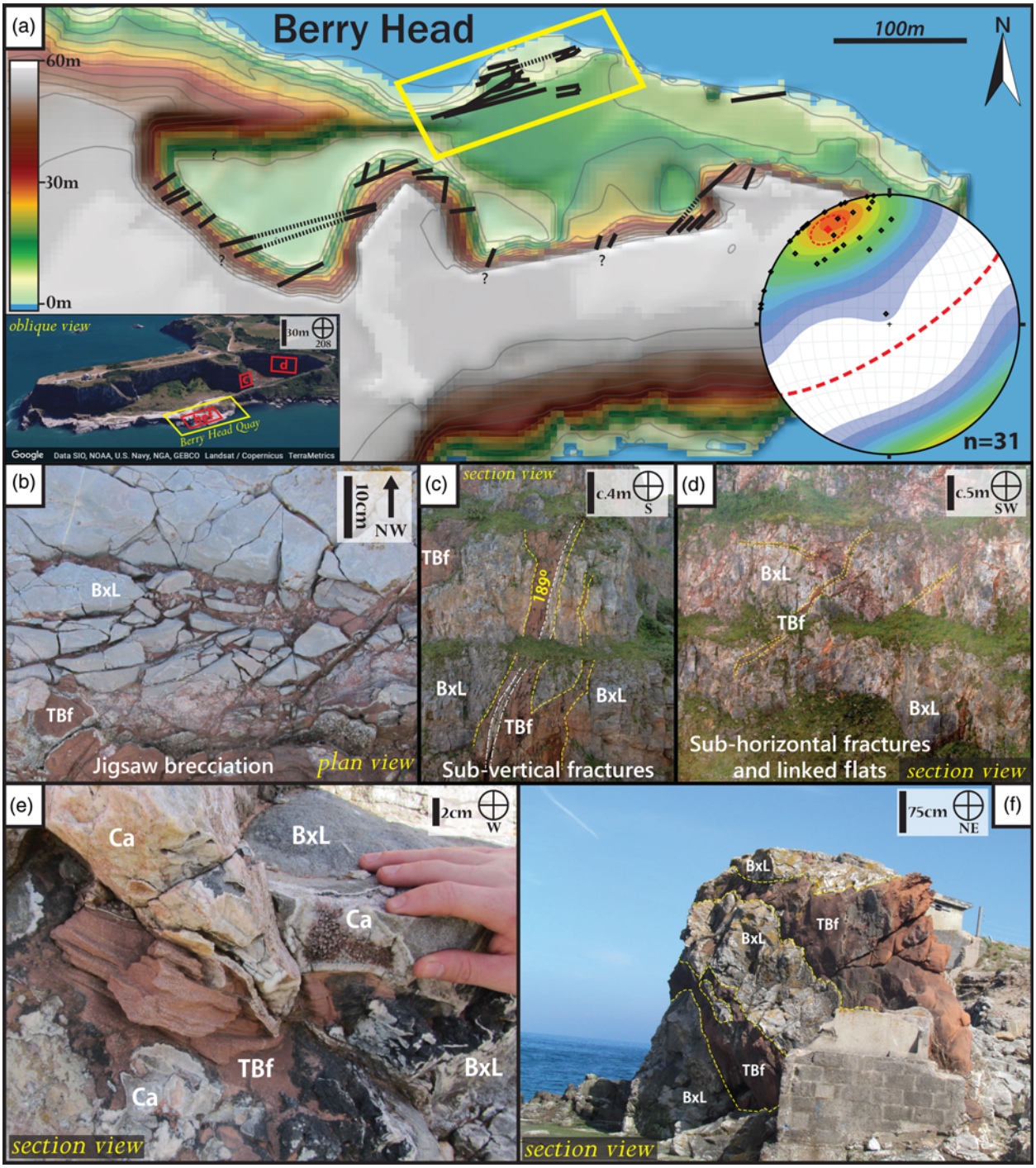

Fig. 5. Field photographs, maps and structural data from Berry Head (for location, see Fig. 2). Field photographs show Brixham Limestone Formation (BxL), faulted and filled by calcite mineralisation (Ca), and Torbay Breccia Formation sandstones (TBf). (**a**) Digitized field sketch map showing locations and orientations of the sediment-filled fractures on headland (black lines) with inset (left) oblique view of Berry Head from Google Earth, with locations labelled. The yellow box is the location of Berry Head Quay. Second inset (right) is a stereonet showing poles to fracture planes and mean cyclographic plane (red) demonstrating the general ENE–WSW strike and SE dip. Base map 5 m digital elevation model (scale shown) generated from Ordnance Survey data provided with permission by Edina Digimap (OS Terrain 5 [XYZ geospatial data], scale 1:10000, tiles sx95nw, updated 3 December 2019, Ordnance Survey (GB), using EDINA Digimap Ordnance Survey Service, https://digimap.edina.ac.uk). (**b**) Plan view of jigsaw breccia in fracture cavity [SX 94418 56714]. (**c**) View of quarry face showing red sandstone infilling and calcite vein development and cross-cutting relationships within vertical fracture cavities in limestone [SX 94296 56619]. (**d**) Section view of sub-horizontal smaller fracture cavities and 'linked-flats' infilled with red sandstone, West Berry Head Quarry [SX 94156 56566]. (**e**) Bedded red sandstone within a small irregular shaped cavity bound by syntaxial sparry calcite growth [SX 94418 56714]. (**f**) Large sandstone-filled subvertical dilatant cavity (right) and bifurcated smaller cavity (left) at Berry Head Quay [SX 94418 56714].

observed in the cliffs with an aperture of 14 m, dipping steeply north (Fig. 4a, b). It cross-cuts a small, south-dipping Variscan thrust that emplaces the Brixham Limestone Formation over rocks of the younger Saltern Cove Formation. The limestone hanging wall of the thrust fault has undergone dissolution at the intersection between the thrust and normal fault. Calcite-bearing vugs (*c.* 2–15 cm) have developed here (Fig. 4f), some of which have been filled geopetally by well-bedded red sandstone. A large limestone clast lies suspended in a matrix of zoned, sub-horizontally bedded red sandstones (Fig. 4a, c), suggesting that the emplacement of the block was contemporaneous with the infilling by red sediments; it appears to have fallen downwards into the cavity from the hanging

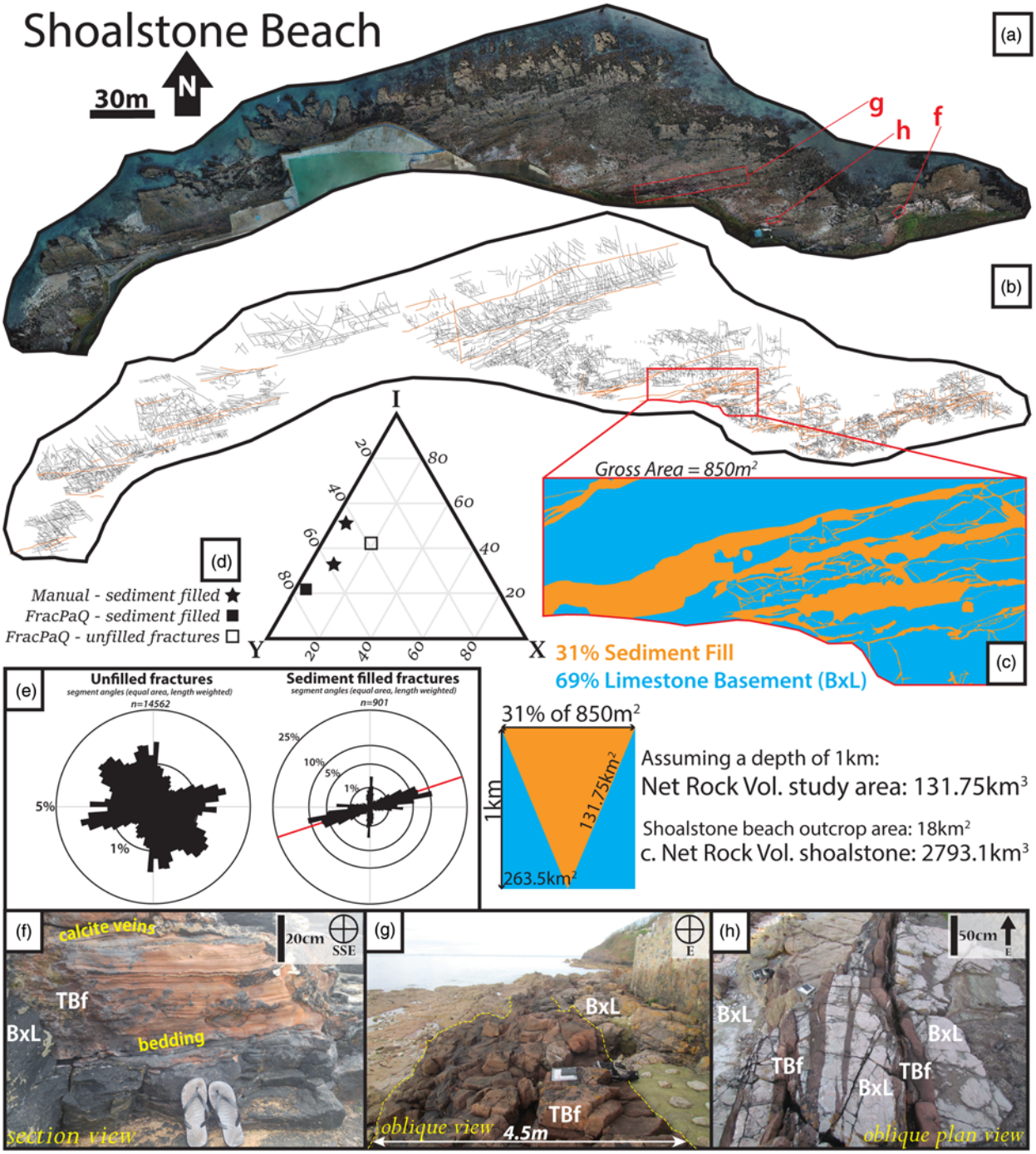

Fig. 6. Orthorectified outcrop images and trace maps, data and field photographs from Shoalstone Beach (for location, see Fig. 2). Field photographs show Brixham Limestone Formation (BxL), faulted and filled by Torbay Breccia Formation sandstones (TBf). (**a**) Virtual outcrop model in which smallest structures resolvable are 1.5–2.5 cm. (**b**) Interpreted fracture trace map. Sediment-filled fractures in orange, unfilled fractures in black. (**c**) Sediment-filled fracture volume map interpreted from within well-exposed selected area shown. Note the irregularity of apertures and traces. A summary of fracture volume estimates is also given; for more information, see Appendix A (Supplementary Material). (**d**) Fracture topology plot of fracture node types showing connectivity (Sanderson and Nixon 2015). Manual and automated (Healy *et al.* 2017) analyses show that both the unfilled and filled fractures are well connected. (**e**) Rose diagrams of fracture segment strike angles generated using the FracPaQ MatLab toolbox, with the average strike in red, showing that sediment-filled fractures are strongly orientated in ENE–WSW and north–south orientations. (**f**) Section view of well-bedded sandstone fracture fill and calcite veining from east of Shoalstone Beach [SX 93834 56770]. (**g**) View of single fracture *c.* 4.5 m in aperture filled with a uniform, homogenous unbedded red sandstone [SX 93696 56789]. (**h**) Interconnected fracture network filled with homogenous red sandstone with no calcite veins lining the wall rock contacts [SX 93775 56780].

wall of the pre-existing thrust. The infilled cavity also contains entrained volcanic material (Fig. 4d, e).

Dilatant fault and fracture corridors

Sub-parallel corridors tens to hundreds of metres wide are best exposed in plan view at Shoalstone Beach and in cross-section at Berry Head Quarry (Fig. 2; Richter 1966; Wall and Jenkyns 2004; Woodcock *et al.* 2014). Other important, though less well-developed, examples occur at Hope's Nose. These fractures typically have apertures of 5–15 cm, but have been observed as narrow as a few millimetres and as wide as 4.5 m.

At Berry Head Quarry [SX 94293 56615] (Fig. 5a), the excavated Mid Devonian limestone walls are up to 60 m high, with a single

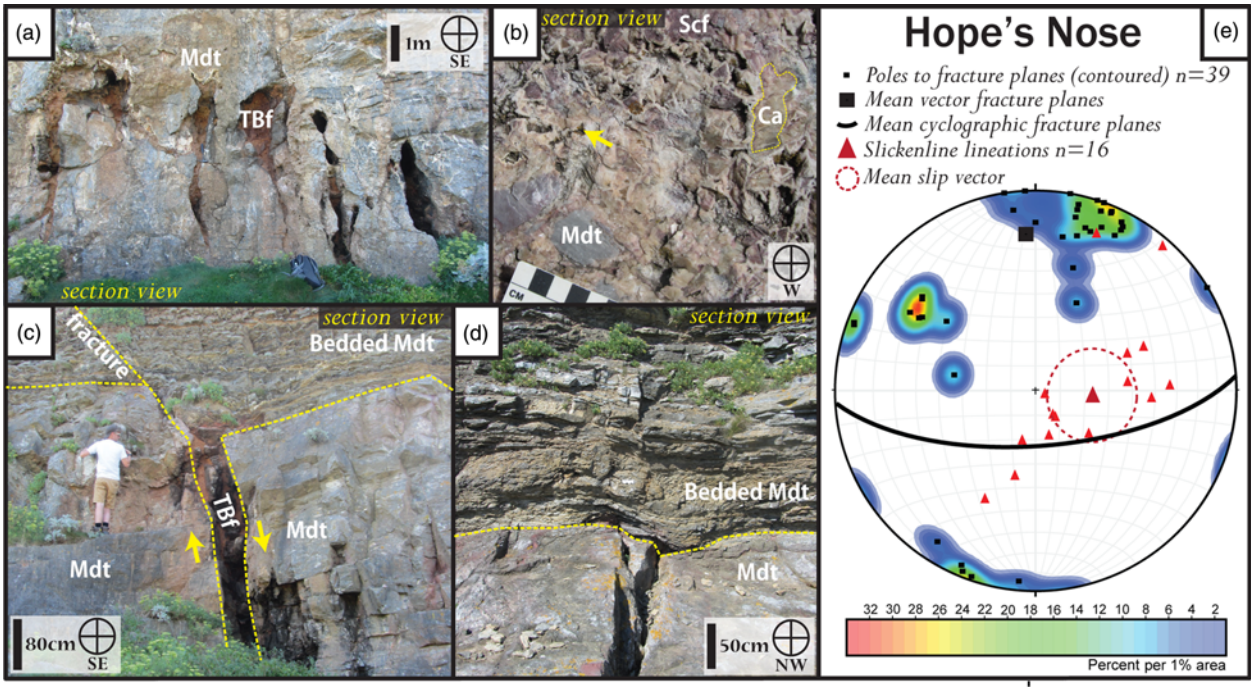

Fig. 7. Field photographs and structural data from Hope's Nose, showing Meadfoot Group deposits (Mdt), fractured and filled by Torbay Breccia Formation sandstones (TBf), calcite mineralisation (Ca), and Saltern Cove Formation mudstones (Scf). (**a**) Section view of red sandstone-filled, lozenge-shaped subvertical fracture cavities showing minor dissolution of the limestone host rock and early karstification prior to the deposition of the infill [SX 94932 63666]. (**b**) Multiphase mineralized breccia. Clasts include limestone, mudstone and earlier brecciated calcite, cemented by secondary calcite and darker ore minerals (arrowed). (**c**) Section view of 'fracture stratigraphy' showing dilatant fracturing in thickly bedded limestones below and shallower dipping narrow shear fracture in thinly bedded mudstones above [SX 94942 63705]. (**d**) Section view of forced fold in finer bedded units. (**e**) Stereonet showing poles to fracture planes and slickenline lineations from Hope's Nose, with mean plane and vector data shown in red [SX 94952 63634].

shelf exposure of cliff section 0.9 km long. Twenty-six subvertical sediment-filled fractures trending either NNE–SSW or ENE–WSW are seen here cutting homogenous massive limestones. No filled fissure tip is observed, with fractures extending vertically over many tens of metres with little systematic change in aperture. Despite having seemingly constant apertures over vertical distances of up to 60 m, the walls of the fracture cavities are locally irregular, with many large angular asperities and entrained blocks of brecciated wall rocks (Fig. 5b, d). These features, together with the lack of any noticeable lateral offset of bedding in the surrounding limestones, indicates that these are predominantly tensile (mode I) opening fractures. At the western end of the quarry, a number of moderately dipping (*c.* 40°) sediment-filled cavities are also exposed linking into vertical fractures (low-angle linkages in Fig. 5d).

At the seafront quay, *c.* 150 m north of the main quarry, five bifurcating and linked sediment-filled fractures occur with apertures up to 40 cm (Fig. 5a – yellow box, e, f). By tracing these fractures along-strike to the equivalent set seen in the quarry walls, we can infer that these fractures are at least 500 m long and show little evidence of narrowing or tipping out laterally, indicating a still larger fracture trace length. A minority of the exposed margins of these fractures appear to have been smoothed. These are interpreted as possible local karst weathering features (Dubois *et al.* 2014). This suggests that these cavities were open close to the surface and were permeable to fluids prior to infilling. Note, however, that the evidence for dissolution is generally limited and that the vast majority of exposed fracture walls feature angular to sub-angular asperities, which can be matched exactly to the opposing fault walls, along with textures such as jigsaw brecciation, which would not be preserved if dissolution had widely affected the fracture surfaces.

A large 700 m long wave-cut platform occurs at Shoalstone Beach, NE of Brixham harbour [SX 93608 56816] (Figs 2 and 6; Richter 1966). Here, an exceptional 2D plan view of sediment-filled fracture networks is exposed cutting Mid Devonian limestones (Fig. 6a–h). As in previous locations, shear offsets of bedding are minimal and the fractures are almost entirely dilational mode I features. Previous researchers have noted that the subvertical fissures occur here in two sets (Richter 1966). An older, paler coloured ENE–WSW set is cross-cut by younger, darker north–south set (Fig. 6f–h). These relative age relationships are typical of the Tor Bay region as a whole and, given the exceptional exposure, this locality can be regarded as the type locality for these sediment-filled fractures.

At Hope's Nose, Mid Devonian reef limestones are cut by irregular sediment- and calcite-filled faults and rare sulfide mineralized fault breccias (Fig. 7a, b). Several faults show a stratigraphic control, where the mode of failure changes within different host units (e.g. Fig. 7c, d). For example, where thicker bedded, more competent limestones are offset, the fault is dilatant (mode I) with a wide aperture (up to 65 cm) filled with sediment. Traced upwards into the directly overlying finer bedded limestones and tuffs, the fault shallows in dip by 20° and becomes a narrower shear fracture (modes II/III) (Fig. 7c). This section of the fault contains breccia and slickenlines, which indicates a normal shear sense (Fig. 7e). In some cases, blind faults are observed to have generated open forced folds directly above the propagating fault tip (Fig. 7d). The fracture sets at Hope's Nose show cross-cutting relationships opposite to those seen in the rest of Tor Bay – that is, sets of (unfilled) north–south fractures here are cut by (sediment- and breccia-filled) east–west faults. These east–west structures show brecciation of mineral fills, suggesting that there was later local fault reactivation here, which may help to explain the difference in percolating fluid chemistries at Hope's Nose described by Shepard *et al.* (2005). Once again, a minority of fractures at Hope's Nose show smoothing of the cavity walls and apparent locally widened apertures (e.g. Fig. 7a), suggesting some minor karstification prior to sediment infilling.

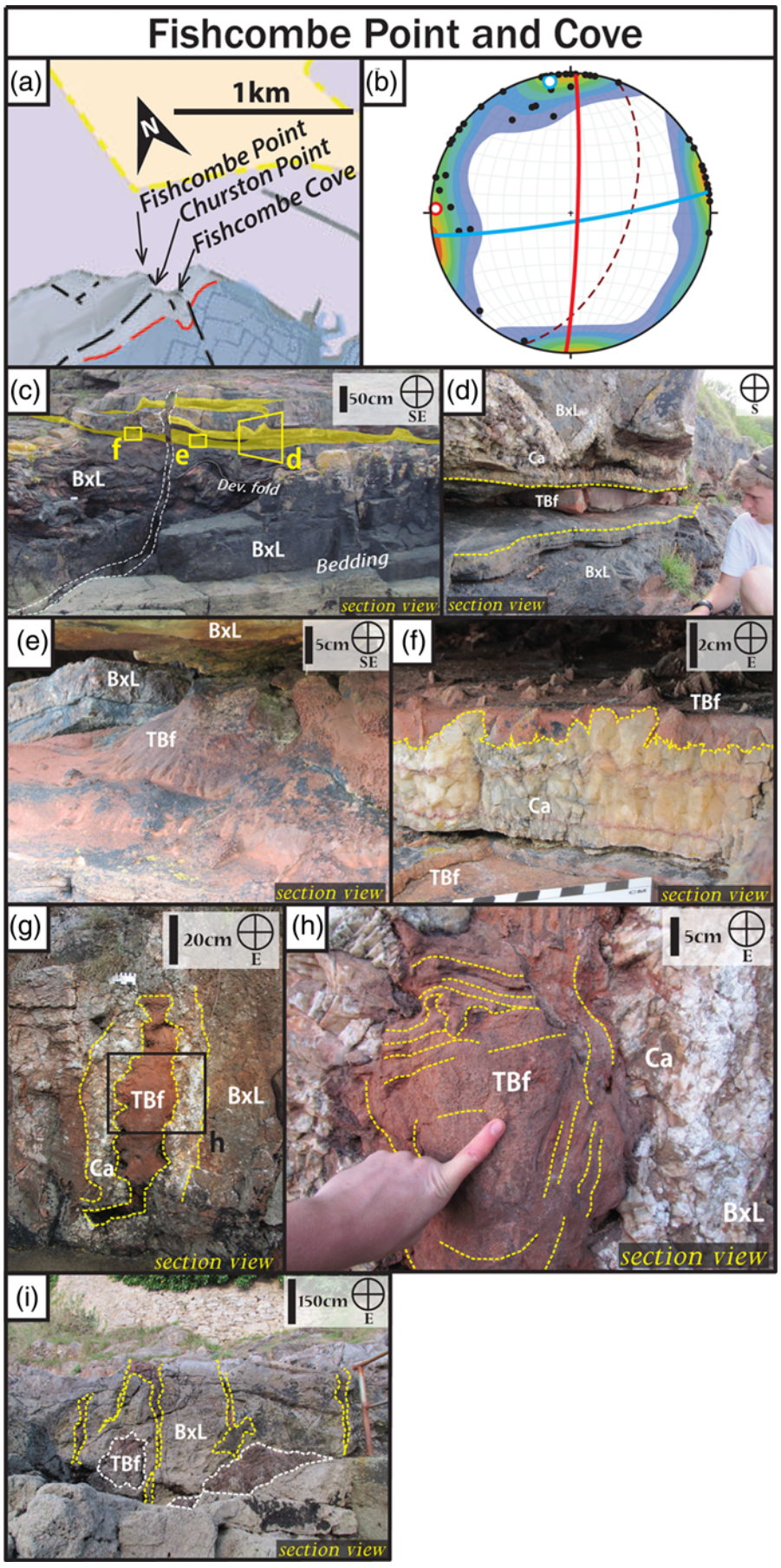

Fig. 8. Field photographs of fissure fills from key outcrops around Fishcombe Point and Fishcombe Cove. Field photographs show Brixham Limestone Formation (BxL), faulted and filled by calcite mineralisation (Ca), and Torbay Breccia Formation sandstones (TBf). (**a**) Local geological map and (**b**) stereonet showing poles to sediment-filled fracture planes for Elberry and Fishcombe, demonstrating east–west and north–south trends as seen in the mean cyclographic planes (north–south in red, east–west in blue); the dark red dashed line corresponds to the large fault at Fishcombe Cove. For key to geological map, see Figure 2. (**c**) Section view of subvertical sediment-filled fault cavity at Fishcombe Point (white lines) and two sets of intersecting sub-horizontal fault cavities (highlighted in yellow). Host rocks are folded Devonian limestones and interstitial mudstones of the Brixham Limestone Formation. Locations of parts (d–f) are also shown [SX 91825 57062]. (**d**) Section view of horizontal fracture cavities showing the relationships between calcite mineralization, minor limestone dissolution and sediment infilling. (**e**) Sand-volcano structures at the intersection of vertical and horizontal fractures. Note the conical shape and central vent and apparent fingering of sediment downslope. (**f**) Section view of horizontal cavity partially filled with red siltstone–sandstone, with the tips of scalar scalenohedral calcite crystals poking through the top surface. (**g**) Section view of large red sandstone-filled cavity with calcite lining at Fishcombe Cove. Location of part (h) is shown by the black box [SX 91979 56929]. (**h**) Close up of red sandstone-filled fracture cavity in part (g), bound by thick calcite veins. Sediment is bedded showing geopetally inclined and horizontal beds in addition to a single well-developed flame structure, all highlighted in yellow. (**i**) View of cross-cutting red sandstone-filled fractures at Fishcombe Cove, younger north–south set picked out in white, older east–west set highlighted in yellow [SX 91976 56949].

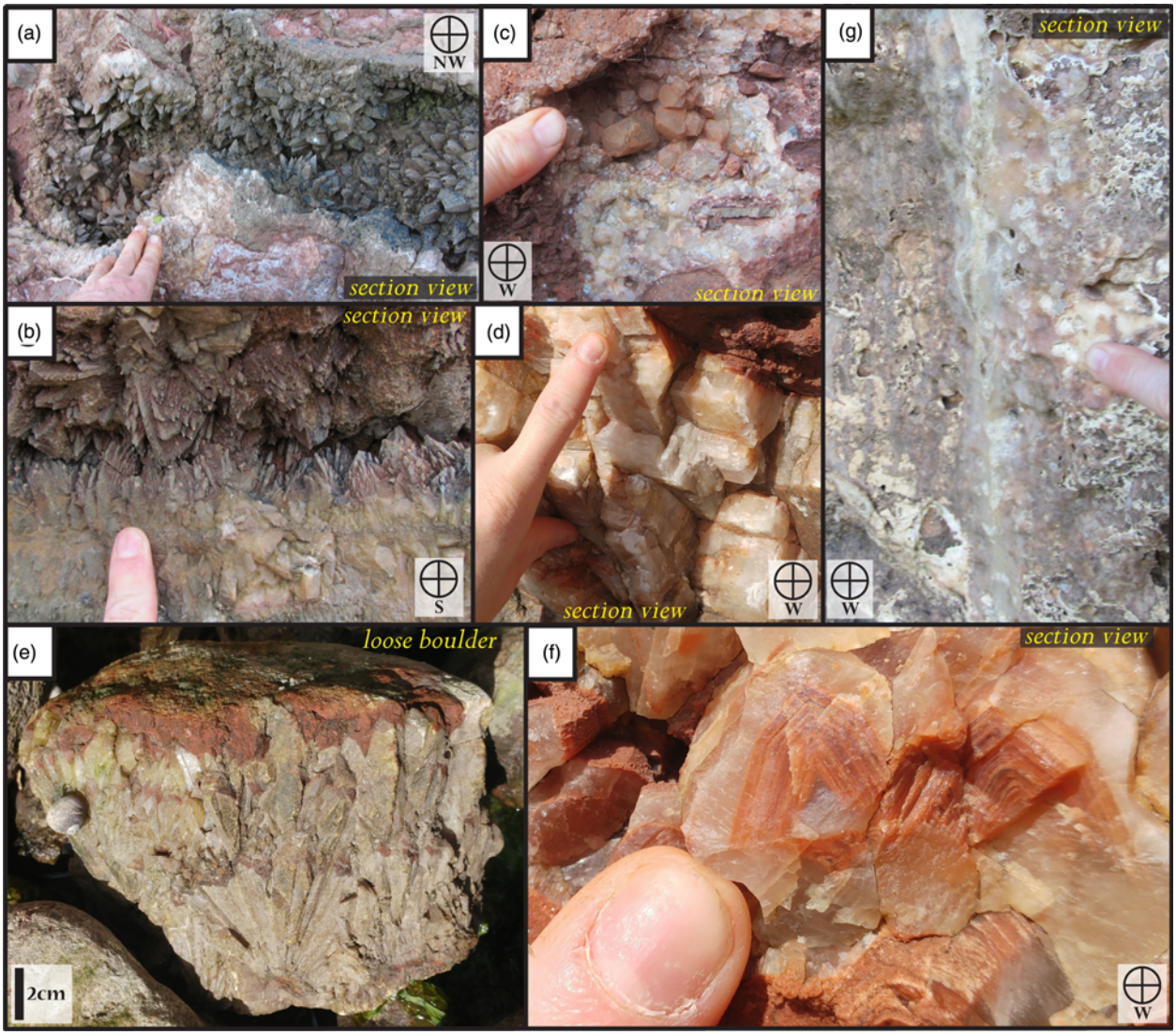

Fig. 9. Field photographs of types of calcite mineralization found in fracture cavities around Tor Bay. (**a**) Simple scalenohedral (dog-tooth spar) calcite, Crystal Cove [SX 89615 58018]. (**b**) Complex scalar scalenohedral calcites growing in a sub-horizontal fracture cavity, Fishcombe Point [SX 91828 57061]. (**c**) Rhombohedral (nail-head spar) sparry calcite, Crystal Cove [SX 89615 58018]. (**d**) Euhedral cubic calcites, Crystal Cove [SX 89586 57977]. (**e**) Splaying 'plumose' calcites later partially filled with sandstone in a loose boulder found near Broadsands Beach [SX 89615 58018]. (**f**) Colour zonation in individual calcite crystals showing variations in hematite content, Crystal Cove [SX 89586 57977]. (**g**) Travertine mineralization, Hope's Nose quarry [SX 94924 63660].

Sub-horizontal forms

Where present, sub-horizontal fracture cavities are usually associated with large vertical faults and fractures. They have previously been referred to as Liassic veins and sedimentary sills (Smith 1952; Richter 1966; Peterson 1967). At Fishcombe Point [SX 91843 57053] (Fig. 8a–d), two small horizontal, partially sediment-filled cavities occur in Mid Devonian limestone with exceptionally well-developed fractal scalenohedral calcite crystals, which line the cavity walls (Fig. 8c–f). These horizontal cavities link into a large (3–17 cm wide, >10 m long) vertical sediment-filled fracture, progressively thinning away from it until they eventually pinch out (Fig. 8c). The horizontal cavities are partially filled by a red homogenous sediment continuous with the sediment fills in the vertical fractures, although it is much finer grained (20–50 v. 250–1000 μm) (Fig. 8d–f). These horizontal cavities are sub-parallel to the pre-existing bedding in the limestone basement (Fig. 8c) and feature locally smoothed cavity walls, indicating that some minor dissolution has occurred during cavity creation (Dubois *et al.* 2014).

Irregular cavity forms

Cavernous carbonate-hosted voids are subordinate features compared with the other forms of fill and are morphologically diverse. At Fishcombe Cove [SX 91979 56942] (Fig. 2), the coastal exposures host a densely packed network of steeply dipping, sediment-filled fractures trending NNE–SSW and east–west (Fig. 8b, i), which show the same cross-cutting relationships as seen at Shoalstone Beach. Less than 10 m east along the coast, a near spherical fracture cavity up to 2 m in diameter occurs and is filled with homogenous, unbedded Permian sandstone. At Fishcombe Point, a series of small 20 cm wide sediment-filled fractures are connected to a number of irregular lozenge-shaped, low aspect ratio (cave-like) cavities (1.7 × 0.5 m) lined with calcite (*c.* 10 cm thick) and filled with bedded Permian sandstone (Fig. 8g, h).

Infills: nature and processes

The intimately associated sediment and calcite fills found associated with faults and fractures in the Tor Bay area must have formed close

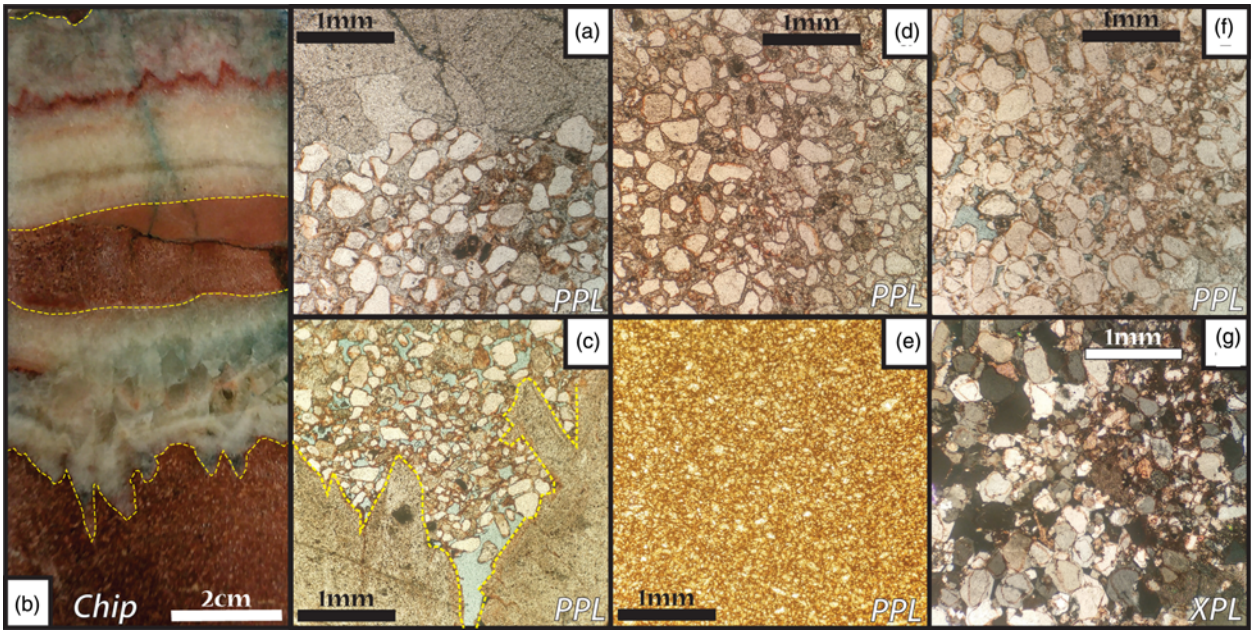

Fig. 10. Thin section photomicrographs of sediment infills. (**a**) Plane-polarized light (PPL) image of sub-rounded red sandstone grains in contact with a calcite vein. Quartz sand grains are coated by a thin rim of hematite. The calcite vein grows in optical continuity with the sandstone cement. (**b**) Thin section chip from a fracture fill at Shoalstone Beach showing the multiphase calcite vein–sediment infilling relationships. (**c**) PPL image of red sandstone infilling gap between two scalenohedral calcite crystals. Note the lack of compaction and high porosity (blue stain). (**d**) PPL image of heavily cemented red sandstone infilling a fracture cavity and showing the paucity of contact points between grains. (**e**) PPL image of fine-grained red silt from sub-horizontal cavity, consisting of material probably elutriated from a nearby vertical sandstone-filled fracture. (**f**) PPL image of cockade-style quartz mineralization of individual grains with intergranular porosity (blue). Rounded quartz grains with a thin hematite coating are enclosed by quartz cement growing in optical continuity with the clastic grains. (g) Cross-polarization image of part (**f**) highlighting the optical continuity of the cockade-style quartz cement surrounding each quartz grain, which are separated by a thin hematite coating.

to the surface based on their proximity to the regional unconformity and the close lithological similarity of the sediment fills to the immediately overlying basal Permian strata.

Mineral fills

Fracture walls are typically lined by sparry calcite fills, which vary significantly in size and morphology from millimetre-thick blocky to metre-thick coarse crystalline spars (Figs 5e, 8d, f and 9a–g). Where sediment fills are present, the veins are normally a few centimetres thick and typically occupy <10–15% of the fracture volume. The calcites are mostly milky white, but dark grey fills are locally developed containing impurities such as carbon or fine iron oxide. Thick sparry calcite veins are consistently syntaxial and grow inwards from the cavity walls (Fig. 9a–f). The associated sediment fills are commonly cross-cut by smaller, younger calcite veins (e.g. Fig. 10b) and new fissure cavities may be present in the infilling sandstone, which are also lined by crystalline calcite (e.g. Fig. 3c, f).

A variety of crystalline calcite forms are observed (Fig. 9), including: scalenohedral (dog-tooth spar) (Fig. 9a); a delicate fractal scalenohedral variety (Fig. 9b); rhombohedral (nail-head spar) (Fig. 9c); fine-grained and sheeted (Fig. 9g); dendritic (Fig. 9e); millimetre- to centimetre-scale stalactites and blocky calcite (Fig. 9d). Fibrous forms are largely absent, except as slickenfibres developed on larger fault surfaces (e.g. Fig. 3d).

Syntaxial cavity-filling textures are best displayed by the scalenohedral and rhombohedral forms (Figs 4f, 8d, f–h, 9a–f and 10b). Both types are known to form in near-surface environments (e.g. García Carmona *et al.* 2003; Milodowski *et al.* 2018) and the lack of mixed calcite morphologies in single fractures suggests that the fluid compositions, water depth and/or temperature may have fluctuated during fissure filling.

Small amounts (<1 cm thick) of fine and sheeted calcite – interpreted to be travertine and flowstone – are seen lining cavity walls in a minority of locations (e.g. Hope's Nose, Fishcombe Point) (Fig. 9g). These features suggest that a limited degree of karstification may have affected some of the open fractures, which also show evidence for minor dissolution (smoothing) along the cavity walls. These karstified fractures can be distinguished from the effects of later Cenozoic–Recent weathering because they are partially covered by Permian sandstone infills.

Calcite textures are consistently growth-zoned, with large scalenohedral calcites commonly showing orange bands parallel to the crystal faces (e.g. Fig. 9f). Colour zonations like this are thought to be controlled by small fluctuations in fluid conditions/chemistry (Paquette *et al.* 1993; Guoyi *et al.* 1995; Milodowski *et al.* 2018). The bright orange stained zones/bands within the calcite crystals probably formed as a result of the enrichment of iron oxides in the mineralizing fluids, which were then precipitated as thin hematite coatings and trapped as iron-rich fluid inclusions (Milodowski *et al.* 2018). More generally, the syntaxial calcites show a marked coarsening-inwards texture (Figs 9a–f and 10b). Multiple sequences of calcite growth from a single wall rock interface are locally developed, with up to three or four bands of coarsening-inwards calcite within a single vein (e.g. Fig. 10b). This is probably due to the repeated pulsing of fluids through the open fracture systems, each generating a renewed phase of mineralization.

Sedimentary fills

Most fills in subvertical faults and fractures are consolidated red sandstones consisting of well-rounded, medium to coarse grains (100–200 μm) of quartz coated in a thin layer of hematite (Fig. 10a–e; Richter 1966). The grains are exceptionally well sorted and most of the sands are homogeneous, structureless and massive (Fig. 10d,

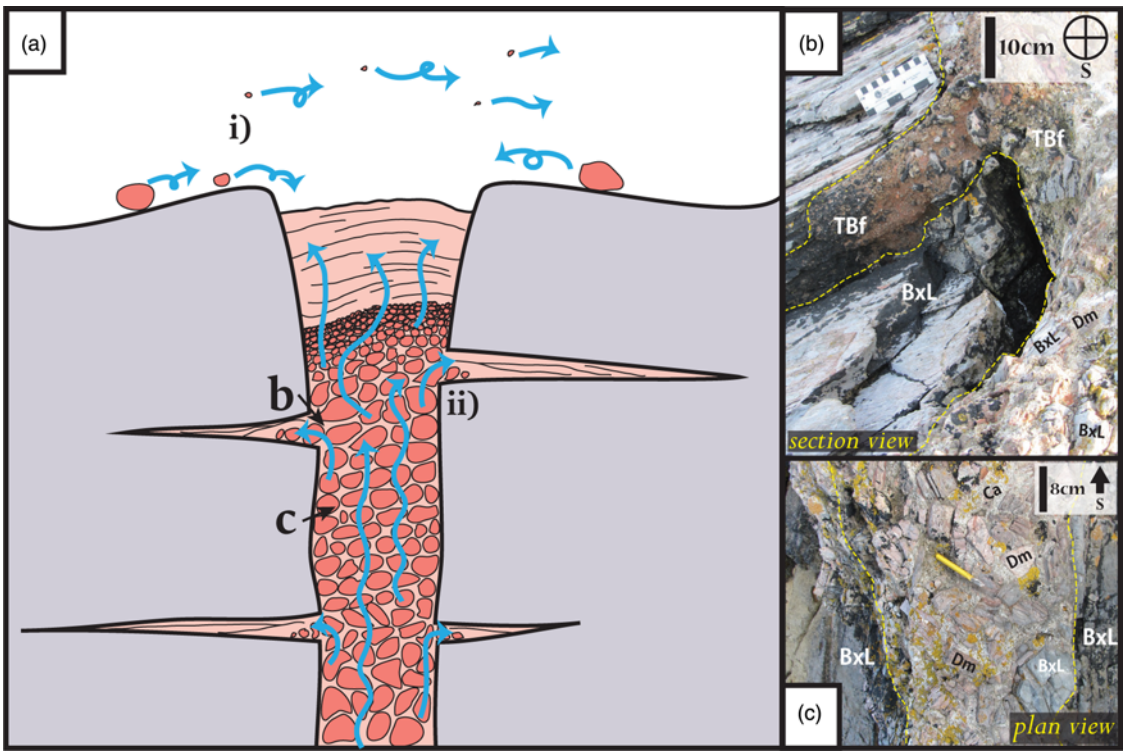

Fig. 11. Fissure-fill elutriation and emplacement sorting processes. Field photographs show Brixham Limestone Formation (BxL), faulted and filled by calcite mineralisation (Ca), Torbay Breccia Formation sandstones (TBf), and clasts of undifferentiated Devonian mudstones (Dm). (**a**) Illustration of near-surface fault architectures and the sorting of unconsolidated infills by fluid flow. (i) Emplacement sorting process where fine material is held in suspension by a fluid and is unable to enter the fracture system, while coarser material rolling around on the palaeosurface is able to fall in. (ii) Elutriation of finer sediment by fluid percolating vertically through the fracture-hosted unconsolidated sediment. Coarser material is held in, or falls out of, suspension, whereas fine material is winnowed out. This fine material is then either deposited where the fluid velocity drops in horizontal or dead-end fractures, or is expelled at the palaeosurface. (**b**) Section view of subvertical to sub-horizontal filled fracture linkage showing fining of the fill in the horizontal fracture away from the vertical cavity. Taken at Fishcombe Cove [SX 92021 56996]. (**c**) Plan view of subvertical fracture in part (b) showing cockade-style calcite mineralization around angular clasts of Devonian mudstone and Brixham Limestone (BxL). The host rock is Brixham Limestone, suggesting the upwards migration of older Devonian mudstone clasts in the cavity. Note the near-uniform clast size and lack of fines despite the proximity to the fine red sedimentary material shown in part (b). BxL, Brixham Limestone; Dm, Devonian mudstone.

e). Bedding, where present, is defined by small variations in grain size and/or by thin laminations of fine silt (Figs 3e, 4c, 5e, 6f and 8h). A proportion of the original porosity in the sediment fills is occluded by mineral cement, but open porosities of up to 10% are common (e.g. Fig. 10c) and locally reach 35%.

In most of the Tor Bay area, fills in the older east–west set of fissures are calcite-cemented, with a great deal of associated calcite veining, whereas the fills in the younger north–south set also feature regions of quartz cement in addition to lesser amounts of calcite (Richter 1966). It is not certain whether this reflects a change in the depositional conditions, but in every other respect the fissures are identical. Where calcite cements are present in the sediments, they grow in optical continuity with large calcite crystals in adjacent mineral fills (Fig. 10a). Where quartz cements are present in the sediment fills of north–south fractures, they are seen to grow in optical continuity with the clastic quartz grains they enclose (Fig. 10f, g), which can be recognized by a thin coating of hematite. Collectively, all of these features suggest that fissure-hosted sedimentation, cementation and calcite mineralization were all contemporaneous.

Further evidence for this contemporaneity comes from the preservation of striking pyramidal piles of sandstone–siltstone within large vertical fault fills and fractures (Fig. 3e). At Crystal Cove, hundreds of these red sediment pyramids can be seen in cross-section within a large calcite-lined north–south fault cavity. They vary in size from millimetres to tens of centimetres across and, in many places, preserve shallowly dipping bedding laminations in the centre of the pyramid, progressively steepening towards the margins (Fig. 3e). Similar features have been described by Woodcock *et al.* (2014) and are thought to represent geopetal accumulations of sediment that have been washed into open, partially mineralized fault cavities and piled up on any asperities or fallen clasts of wall rock that were present.

Chaotic breccia fills up to several metres wide are found in many sediment-filled fissures around Tor Bay. The most common type consists of irregularly oriented, angular clasts of wall rock limestone that show no evidence of attrition or rounding (e.g. Figs 4a, c, 7b and 11c). These are thought to have formed by collapse of the wall rock into open fissures (Woodcock *et al.* 2014). Locally, jigsaw-type breccias are developed where clast fragments are seen to be only slightly displaced from their original position (e.g. Fig. 5b). In all cases, the breccia clasts are held in a uniform matrix of red sandstone, suggesting that brecciation occurs coevally with sediment infilling.

A few more exotic fills are found locally in some larger fracture systems. At Saltern Cove, an irregular zone of breccia fill includes clasts of tephra with associated copper and lead mineralization, enclosed in a matrix of fine-grained red sandstone (Fig. 4d, e). Clasts are of orange-coloured tuff and copper-rich clasts of volcanic ejecta. The sandstone matrix here preserves bedding laminations that wrap around the volcaniclastic clasts, suggesting that they were already lithified before being incorporated into an open cavity along

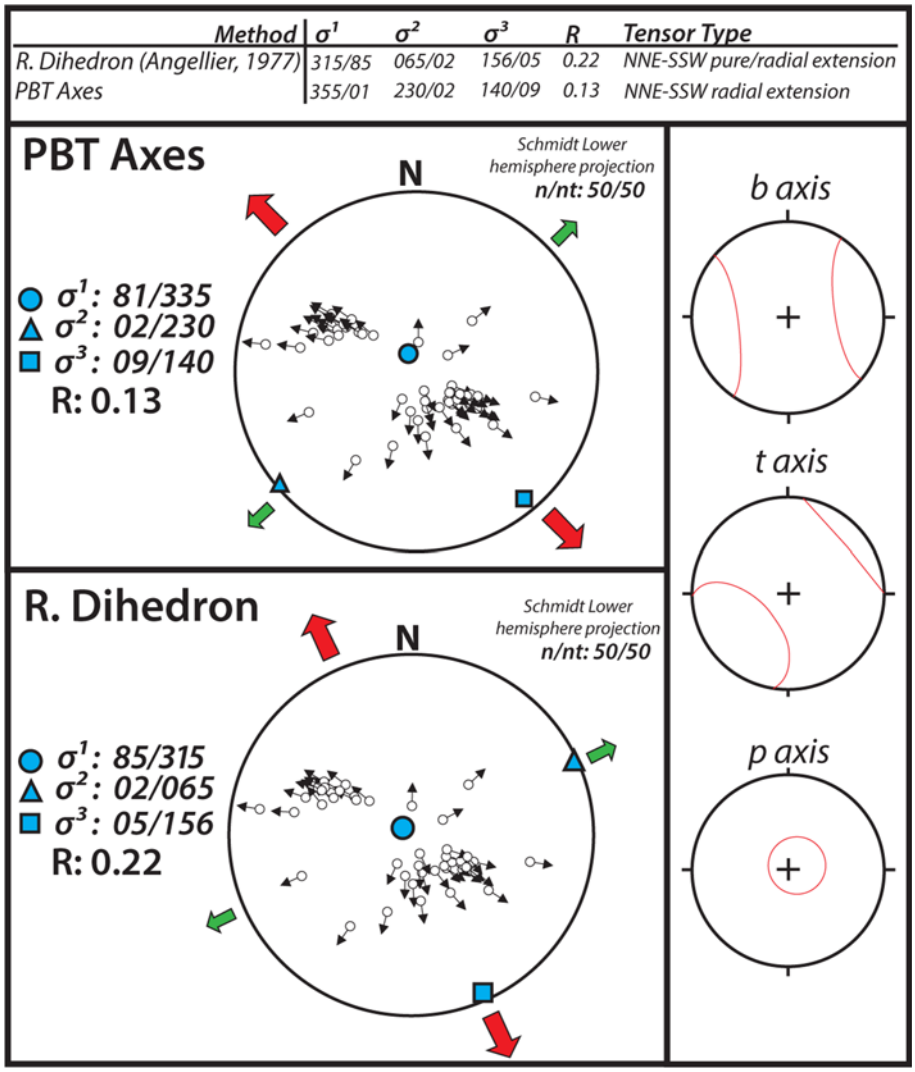

Fig. 12. Palaeostress analysis of slip vectors (slickenlines) from major fault planes using WinTensor (Delvaux *et al.* 1995; Angelier and Mechler 1997). Results tabulated in upper panel and illustrated in stereonet projections in the lower panel.

with the unlithified sand. This volcanic material may have originated from the Late Devonian interstitial basaltic tuffs within the Saltern Cove Formation, reworked at the surface and emplaced into the cavity (Smith 1952). The vertical and horizontal zonation of the sediment infilling the large normal fault cavity here further suggests that this fault-related fissure was repeatedly and cyclically reactivated, dilating and filling iteratively over time.

At Fishcombe Point and SE of Fishcombe Cove, the sedimentary fills in sub-horizontal fractures are finer grained (20–50 μm) than the adjacent vertical fracture fills and show normal grading consistent with deposition from a fluid suspension. This may indicate that these open fractures were regions of lower energy fluid flow, where finer sedimentary material elutriated from the adjacent, faster flowing vertical fracture cavities was deposited (Cox and Munroe 2016). The local development of sand volcanoes close to the intersections of vertical and horizontal cavities (e.g. Fig. 8e) also points to fluid fluxing and elutriation. Along the slopes of the sand volcanoes, interfingering sedimentary structures with slight variations in grain size reveal different depositional events, showing that these probably formed iteratively over many repeated fluid flux events (Fig. 8e).

A large lozenge-shaped sediment fill with an aperture of a few tens of centimetres occurs along the eastern side of Fishcombe Cove (Fig. 8g–i). The fracture is lined by sparry calcite and the infilling sediment hosts an array of sedimentary structures, including cross-bedding and dewatering structures (Fig. 8h). Unusually, the earliest sediment fills here were concentrated along the sides of the cavity in very steep beds, most probably caught against the walls because the majority of the sediment fell deeper into the fault cavity. Once the steep beds met and blocked the fissure, shallowly dipping beds were deposited on top. These beds preserve dewatering and flame structures consistent with periodic fluid fluxing events (Fig. 8h).

Discussion

Our observations indicate that the fracture-hosted cavities in the Devonian limestone basement are fault-related fissures formed at, or within no more than a few hundred metres of, the surface. These cavities have been pervasively infilled by Permian red sediment, with broadly contemporaneous calcite (and minor quartz) mineralization. The near-surface interpretation is predicated on the close spatial association between the occurrence of the red sediment fills and the presence of the regional (early Permian) unconformity. The clastic material either fell, or was washed, into a network of long-lived open, subterranean cavities and was then variably reworked and redistributed by periodic upwards-directed fluid fluxes (Fig. 11). The intimate association between the sediment fills and the calcite-dominated mineral fills suggests that these fluid fluxes are plausibly related to active rifting in the early development of the Portland–Wight Basin.

Karstification v. tectonic fissure formation

Karstification has a significant role in the development of cavity systems in shallow basement carbonates worldwide (Hauselmann

et al. 1999). In the Tor Bay area, large Quaternary cave systems are known within the carbonate basement, such as Kent's Cavern (Lundberg and McFarlane 2007). However, most of the fracture cavities directly associated with Permian sediment and mineral fills in fissured limestone show very angular cavity walls and asperities, with little or no evidence of aperture widening and dissolution (see also the examples discussed by Woodcock *et al.* 2014). The preservation of faults with shear offsets and slickenlines is further evidence of tectonic faulting at the time of open fissure formation. Fifty slickenside lineation measurements and relative displacement senses were subjected to a stress inversion analysis. (Fig. 12). The results suggest that both east–west and north–south structures formed under an extensional radial stress system (vertical $\sigma 1$) with a NNW–SSE primary extensional axis ($\sigma 3$) and an ENE–WSW secondary extensional axis ($\sigma 2$) (Fig. 12). Collectively, these observations suggest that the majority of fissure fills here are of tectonic origin and the extensional stress system shows that they are most likely related to the early stages of Permian rifting and basin formation rather than Variscan contractional deformation. Analogue models of dilatant normal fault systems in carbonates have shown how vertical tensile fissures formed in the near-surface link at depth to inclined hybrid and shear fractures with dilational jogs at intermediate levels (Fig. 1a, b; van Gent *et al.* 2010). Importantly, the NNW–SSE extension direction derived here is consistent with the direction of Permian rifting inferred from onshore and offshore geological studies in SW England (see Shail and Leveridge 2009 and references cited therein).

Mineral filling mechanisms

Mineral zonation and cockade textures (Frenzel and Woodcock 2014 and references cited therein) are widely recognized on micro- to meso-scales, with the best examples preserved at Crystal Cove, Petit Tor Point and Shoalstone Beach. Here, the mineralized fracture cavity fills have individual clasts that are completely surrounded by, and therefore appear to float in, multiple concentric layers of cement (Figs 7b, 10e and 13a). Elongate scalenohedral or rhombohedral calcites surround clasts ranging from single quartz sand grains to large clasts of Devonian wall rock (Figs 10e and 13b). The paucity of contact points between the clasts suggests that the clasts are free to move away from one another. Fractured cockades (e.g. Fig. 13b) are locally preserved, but the more widespread development of uniform overgrowths within and between clasts requires that the mineral cements grew evenly on all sides of each clast at the same rate. Although some of the concentric overgrowths may be the result of a cut effect during sampling, their prevalence across multiple samples and the paucity of contact points between clasts shows that the majority are true cockades. This suggests that they grew either in suspension and/or by repeated accretion and rotation of clasts in an upwards-flowing supersaturated fluid (Fig. 13a, b; Frenzel and Woodcock 2014; Cox and Munroe 2016). More generally, the preservation of such textures indicates that the fracture cavities remained open for significant periods and were subject to episodic fluid fluxes with significant flow velocities. The open nature of the fissures is consistent with filling by red sediment derived from above and the ubiquity of this relationship suggests that complete sealing of mineralized fissures rarely occurred (see discussion in Frenzel and Woodcock 2014).

Crack-seal textures and fibrous calcite fills are preserved widely in dilational calcite veins in the Devonian basement rocks, where they also have a distinct yellow coloration compared with the younger milky white fissure-fill calcites. These older features are widely interpreted to indicate the cyclic build-up of fluid pressures leading to repeated episodes of hydraulic fracturing and mineral precipitation (e.g. Ramsay 1980; Cox and Etheridge 1989). The absence of such features in the later mineralized mode I fractures of

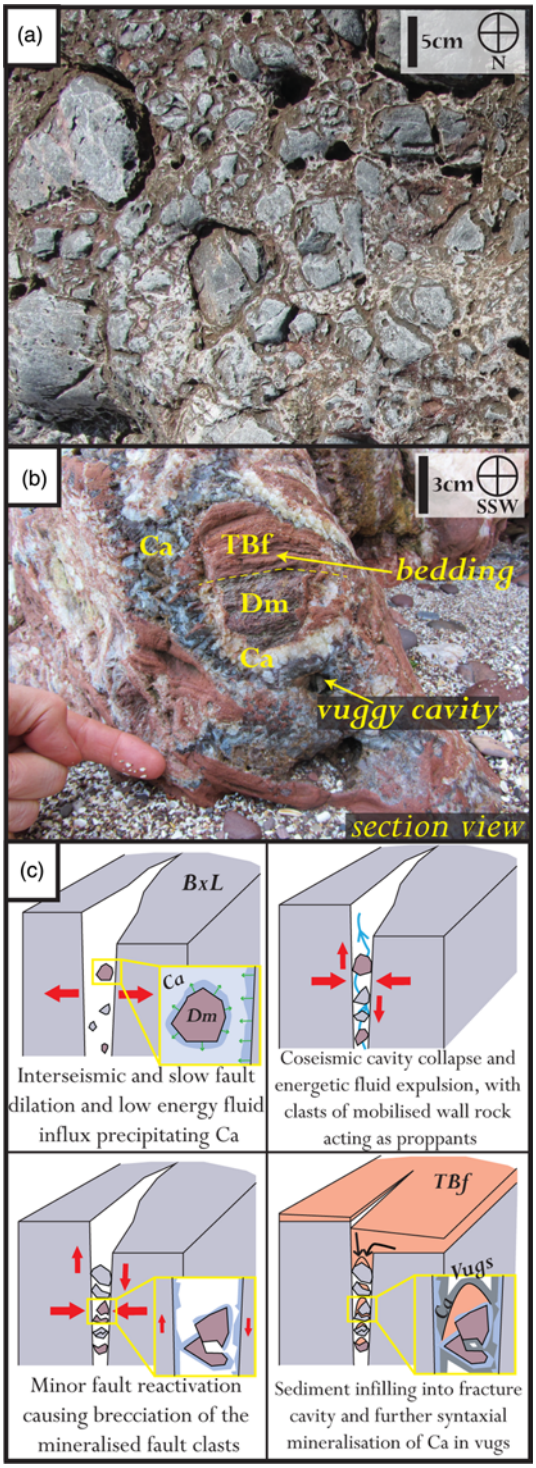

Fig. 13. Examples and models of multiphase breccia formation. Field photographs show fissures fills within the Brixham Limestone Formation (BxL) containing calcite mineralisation (Ca), bedded Torbay Breccia Formation sandstones (TBf), and clasts of undifferentiated Devonian mudstones (Dm). (**a**) Fault breccia from Petit Tor Point displaying cockade-style mineralization with clasts of angular limestone separated by calcite mineralization. This is different from other cockade-style fabrics in Tor Bay because the thickness of calcite veining varies [SX 92649 66144]. (**b**) Section view of fault infill from Crystal Cove showing fractured cockade-style brecciation, mineralization and geopetal sediment infilling around clasts of suspended older wall rock [SX 89541 57918]. (**c**) Panelled illustration of formation of fault infill seen in part (b) from repeated fault movement, fluid flux events and passive sedimentary infilling.

inferred Permian age is consistent with the fissures remaining open or partially open as a result of their near-surface location, meaning that significant build-ups of fluid pressure, which might lead to

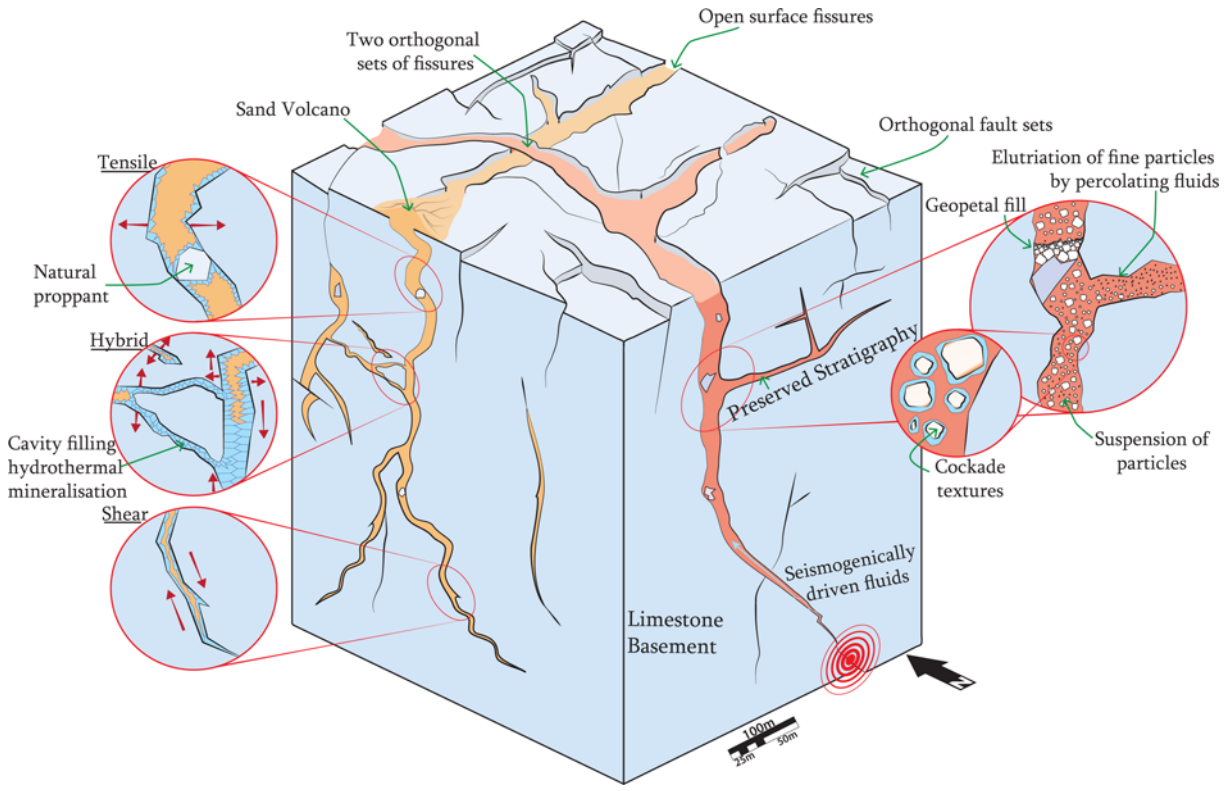

Fig. 14. Schematic synoptic illustration of a typical near-surface, mineral- and sediment-filled fault and fissure system and processes hosted in carbonate basement based on observations in the Tor Bay area.

hydraulic fracturing (i.e. fault valve behaviour; Sibson 1990; Cox and Munroe 2016), did not occur.

Red sediment filling mechanisms

Sediment-filled fractures are commonly referred to as either neptunian dykes or injectites (Richter 1966; Martill and Hudson 1989; Siddoway and Gehrels 2014; Siddoway *et al.* 2019). Sediment that has been driven into a fracture cutting a low-permeability host rock in the subsurface is commonly referred to as an injectite (Hurst *et al.* 2011 and references cited therein). Injectites are generated where overpressure develops in a poorly consolidated uncemented sandstone, leading to hydraulic fracturing in an adjacent (usually) overlying lithology, but they have also been recognized in crystalline basement lithologies beneath unconformities (Siddoway and Gehrels 2014; Holdsworth *et al.* 2020; Siddoway *et al.* 2019). A lack of internal sedimentary structures is a characteristic feature of injectite sediment slurries (Walton and O'Sullivan 1950; Peterson 1967; Walker *et al.* 2013).

There is little evidence for the injection of sediment in the Tor Bay area. Although it is not ubiquitous, horizontal bedding is locally observed within many cavity fills (Figs 3e, 4c, 5e, 6f, 8h and 13b) and the large euhedral, scalenohedral form of the calcite crystals that line the fracture cavities shows that the voids were open before sediment infilling (Figs 5e, 8c–h and 9e). Laminated sediment fills are also associated with a variety of geopetal structures that consistently young upwards and show that sediment progressively filled pre-existing open voids (Figs 3e, 4c, 5e, 6f, 8c–h and 13b). The frequent lack of bedding laminations in many Tor Bay examples may be due to the periodic and repeated upwards percolation of fluids through the sediment-filled fracture systems during and immediately following deposition, but prior to lithification (Fig. 11). This fluid flux could have been sufficient to destroy any sedimentary structures and cause a large-scale sorting/local homogenization effect by elutriating the sediments and removing fines. Close to some of the larger basin-bounding faults, there is evidence of multiple fault movements at the same time as hydrothermal mineralization and sediment deposition. It is certainly conceivable that the repeated opening and closing of fault and fracture cavities in cohesive limestone basement close to the surface would lead to local changes in fluid pressure. Hence it may be that finer silty fractions were forced into open fractures following elutriation (Fig. 11a–c). The result is a mass of sediment that has pervasively invaded any available and connected void space in the limestones below the regional base-Permian unconformity.

Given the evidence for the flux of fluids through the sediment-filled fractures, it seems likely that some sediment was ejected from the fracture system and effused at the surface, but has since been removed due to the erosive nature of the base-Permian unconformity. This would probably appear in the rock record as sand volcanoes, similar to those seen within some horizontal fault cavities (e.g. Fig. 8e). Sand volcanoes are well reported in the rock record (Gill and Kuenen 1957; Rowe 2013), but are more commonly associated with liquefaction processes during seismic shaking, rather than co-seismic fluid flux. Large magnitude earthquakes – such as in Christchurch, New Zealand (2011), Niigata, Japan (1964) and the New Madrid Seismic Zone, USA (1812) – have been shown to produce sand volcanoes at the surface as a result of co-seismic liquefaction processes. However, despite the lack of onshore examples, large offshore submarine mud volcanoes – such as the Bortoluzzi volcano, offshore Calabria, Italy – often sit above major active fault zones and are formed through similar processes (Cuffaro *et al.* 2019).

What drove fluid flow?

Although it is clear that the limestone-hosted fractures formed close to the surface and were open for long time periods, there is also evidence for cyclical, upward fluid fluxing events. Given the tectonic origin of the fissure systems and the clear association with

active Permian rifting, it is likely that the migration of these fluids could be driven by co-seismic slip along larger basin-bounding faults at depth (Sibson *et al.* 1975; Sibson 1981, 1994; Muir-Wood and King 1993). Semi-regular slip events along large faults will lead to changes in the shape and volume of fault voids, driving fluids out and drawing fluids in throughout the connected void network, and suspending or rolling clasts around and precipitating minerals (Figs 13c and 14). Because the architecture of the observed fault voids are often irregular, curvilinear and bifurcated, the opportunity to develop dilational jogs and props is widespread. As the faults accumulate slip, these jogs will open and close, creating and reducing fracture volumes and causing changes in pressure, leading to the mobilization of fluids and suspended sediment throughout the connected cavity network. It is not known whether the fluids involved here were meteoric or hydrothermal – or a mixture of both – and fluid inclusion and stable isotope analyses are required to determine the origins of the host fluids. Either way, a tectonic mechanism related to seismogenesis during rifting seems a plausible driving mechanism.

Implications for long-term fluid transport and storage

As the marginal parts of many rift basins overlie regional erosional unconformities, there is every reason to extrapolate that similar sediment and mineral-filled fissure systems may form anywhere where the basement is strong and cohesive (e.g. massive carbonates, crystalline basement and basalts). Examples of such fills from the geological record have been described in all these rock types (e.g. Angelier and Mechler 1977; Schlische and Ackermann 1995; Beacom *et al.* 1999; Walker *et al.* 2011; Siddoway and Gehrels 2014; Siddoway *et al.* 2019). Good modern examples are seen associated with the Dabbahu Fissure (Affar rift, Ethiopia) (Rowland *et al.* 2007) and the Mid-Atlantic Ridge (Iceland) (Kettermann *et al.* 2019). These modern examples also feature fissures filled with surface detritus (sediment/lava/scree) and are formed along tectonic boundaries (Rowland *et al.* 2007; Kettermann *et al.* 2016, 2019). Similar structures to those studied here, such as zoned calcite mineralization, are also reported in modern fissure systems (De Filippis *et al.* 2012).

As the basement subsides and is buried, the sediment and mineral fills prop open the highly interconnected network of cavities, potentially maintaining the large apertures and connection pathways (Holdsworth *et al.* 2019, 2020). If the sediment within the cavities is largely free of clay due to the effects of elutriation and is well sorted and distributed throughout the fracture network, then it has the potential to preserve a high porosity and permeability, provided that the pore space does not become completely occluded by mineral cement. Although a detailed porosity analysis of the Tor Bay fissures has not been carried out in the present study, optical estimates from thin sections suggest local porosities of 10–35%, which is significantly higher than in the surrounding Devonian limestones. This illustrates that these fracture fills are potentially important sites for the subsurface storage of fluids in hydrocarbon basins, geothermal reservoirs or aquifers.

The drone-based orthorectified virtual outcrop model (Fig. 6a) and fracture trace map (Fig. 6b) from Shoalstone Beach illustrate in plan view the very high interconnectivity of the sediment- and mineral-filled basement fissure systems formed in near-surface settings (Fig. 6a–d, g, h). A fracture topology plot (Fig. 6c; Sanderson and Nixon 2015) shows the connectivity of both the unfilled and sediment-filled fracture networks at Shoalstone Beach, with >1.8 connections per fracture branch (>1 is the threshold for a connected network). All the sampled fracture networks show a dominance of Y-nodes over X- or I-nodes, although the unfilled network has more I-nodes despite the higher number of fractures present. An areal calculation showed that, in fracture corridors such as this, the percentage area of potentially highly permeable sandstone fill locally reaches up to 69%. Further details of the virtual outcrop modelling and analysis, including an attempt to estimate the total volumes of fracture fill, is given in Appendix A.

In the light of these findings, it is important to note that the basal Permian–Triassic unconformities in the southern part of the UK are widely known to be associated with clastic and mineral infills (e.g. Woodcock *et al.* 2014, see their fig. 13). For example, in Pembrokeshire, Carboniferous limestones are cut by large sediment- and mineral-filled faults and fractures formed during the opening of the Bristol Channel Basin. The late Triassic sediment fills here feature cockade textures and geopetal accumulations, whereas the limestones show only minor karstic dissolution and extensive brecciation (Wright *et al.* 2009; Woodcock *et al.* 2014). Arrays of red Triassic to early Jurassic sediment-filled fractures and faults also cut Carboniferous limestones in the Mendips (Williams 1986; Wall and Jenkyns 2004).

Collectively, our observations may explain why the basal Permo-Triassic unconformity and underlying fractured basement are thought to form a significant aquifer and potential geothermal reservoir in the southern British Isles. The unconformity is thought to provide an ingress point for fluids to generate substantial recent karst networks, potentially enabling deep-heat geothermal prospects (Narayan *et al.* 2018 and references cited therein). Faults and fractures with porous fissure fills will probably enhance the penetration of karstifying fluids, augmenting the potential for basement Devonian–Carboniferous limestones to be a significant geothermal reservoir. Fracture attribute and connectivity information collected in field sites, such as the Shoalstone Beach outcrop, could be important in helping to build better predictive fractured reservoir models.

Reactivation and timing relative to other regional events

Apart from the larger basin-bounding fault zones, such as those of Crystal and Saltern coves, there is relatively little evidence for reactivation of the fractures and associated fissure fills. An exception occurs at Hope's Nose. Mineralized fault breccias here are developed in Mid Devonian limestones (Russell 1929; Scrivener *et al.* 1994). These fault breccias trend broadly east–west (090–123°), cross-cutting a set of unfilled north–south fractures. The presence of re-brecciated calcite breccia here (Fig. 7b) shows that the east–west faults and fracture corridors have been reactivated. Dendritic native gold, palladium and hematite mineralization within the re-brecciated fractures is associated with localized acidic fluid alteration of calcite (Russell 1929; Scrivener *et al.* 1994). This chemically diverse, cross-course mineralization has been dated at 236 Ma ± 3 Ma (mid- to late Triassic) using Rb–Sr dating of quartz by Scrivener *et al.* (1994). These researchers suggested that the fluids were basinal brines originating from the Permo-Triassic New Red Sandstone and Aylesbeare mudstones. It is also plausible that they are a distal manifestation of the rifting responsible for the formation of fissures in the region of the Bristol Channel Basin to the NW (Woodcock *et al.* 2014 and references cited therein). Collectively, these observations illustrate that the initiation of the Portland–Wight Basin (Permian) was significantly earlier than the onset of rifting to form the Bristol Channel Basin (Triassic–Jurassic) in SW England.

Conclusions

The geological material found within fracture-hosted cavities in basement rocks below regional unconformities preserves a valuable and under-utilized source of information about early basin histories. The fissure-fill systems formed in the fractured Devonian limestones of the Tor Bay area (Fig. 14) are thought to have formed

during early Permian NNW–SSE rifting linked to early stages in the opening of the offshore Portland–Wight Basin. Cyclical and iterative precipitation of mainly calcite from circulating, possibly upwelling, fluids occurred close to the surface (<1 km depth) in the fissures, plausibly related to repeated seismogenic faulting during rifting. At the same time, clastic sediments and wall rock fragments fell into, or were washed into, the open fault-related fissures from above (Figs 11 and 14). Once incorporated, the sedimentary material in the fissures was commonly repeatedly remobilized, sorted and redistributed by further episodes of fluid circulation throughout the near-surface fissure network. These fractures were effectively propped open by their sediment and mineral fills and also by the inherent irregularity of the cavity walls, preserving their interconnectivity and potential permeability (Fig. 14). This may explain why the basal Permian–Triassic unconformities of southern England, which are known to be widely associated with filled fissures of this kind, are associated with the development of significant regional geothermal reservoirs and aquifers. This is also likely to be the case globally in sub-unconformity settings of this kind.

Acknowledgements This work was undertaken by Kit Hardman as part of an ongoing PhD studentship. The authors thank the members of the structural research group at Durham University for many helpful discussions, most notably Tom Utley and Zach Killingback, and the authors ever-patient partners. Reviewers Cathy Hollis and Nigel Woodcock and Editor Linda Kirstein all made very constructive and helpful suggestions to help improve our paper, which are much appreciated.

Author contributions **KH**: data curation (lead), formal analysis (lead), investigation (lead), writing – original draft (lead); **REH**: conceptualization (lead), investigation (supporting), methodology (supporting), supervision (lead), writing – original draft (supporting), writing – review and editing (lead); **ED**: data curation (supporting), investigation (supporting), software (supporting), supervision (supporting), writing – review and editing (supporting); **KM**: investigation (supporting), methodology (supporting), supervision (supporting), writing – review and editing (supporting).

Funding Fieldwork by KH was in part funded by the Institut Françias de Petrol Grant from the AAPG Grants-in-aid foundation. Additional funding was provided by Hurricane.

Data availability statement All data generated or analysed during this study are included in this published article and its Supplementary files).

Scientific editing by Linda A Kirstein

References

Angelier, J. 1991. Inversion directe et recherche 4-D: comparaison physique et mathematique de deux modes de determination des tenseurs des paleocontraintes en tectonique de failles. *Comptes Rendus d'Académie des Sciences, Serie II*, **312**, 1213–1218.

Angelier, J. and Mechler, P. 1977. Sur une methode graphique de recherche des contraintes principales egalement utilisables en tectonique et en seismologie : la methode des diedres droits. *Bulletin de la Société géologique de France*, **S7-XIX**, 1309–1318, https://doi.org/10.2113/gssgfbull.S7-XIX.6.1309

Arthus-Bertrand, J. 2004. *Earth From Above*. Arthus-Bertrand, Jann.

Arthus-Bertrand, Y. 2020. Yann Arthus-Bertrand | Yann Arthus-Bertrand Photos, www.yannarthusbertrand2.org/

Beacom, L.E., Anderson, T.B. and Holdsworth, R.E. 1999. Using basement-hosted clastic dykes as syn-rifting palaeostress indicators: an example from the basal Stoer Group, northwest Scotland. *Geological Magazine*, **136**, 301–310, https://doi.org/10.1017/S0016756899002605

Bott, M.H.P. 1959. The mechanics of oblique slip faulting. *Geological Magazine*, **XCVI**, 109–117, https://doi.org/10.1017/S0016756800059987

British Geological Survery. 2004. *Torquay. England and Wales Sheet 350 (Solid and Drift Geology. 1:50 000)*. Keyworth, Nottingham: British Geological Survey.

Coward, M.P. and McClay, K.R. 1983. Thrust tectonics of S Devon. *Journal of the Geological Society, London*, **140**, 215–228, https://doi.org/10.1144/gsjgs.140.2.0215

Cox, S.F. and Etheridge, M.A. 1989. Coupled grain-scale dilatancy and mass transfer during deformation at high fluid pressures: examples from Mount Lyell, Tasmania. *Journal of Structural Geology*, **11**, 147–162.

Cox, S.F. and Munroe, S.M. 2016. Breccia formation by particle fluidization in fault zones: implications for transitory, rupture-controlled fluid flow regimes in hydrothermal systems. *American Journal of Science*, **316**, 241–278, https://doi.org/10.2475/03.2016.02

Cuffaro, M., Billi, A. *et al.* 2019. The Bortoluzzi mud volcano (Ionian Sea, Italy) and its potential for tracking the seismic cycle of active faults. *Solid Earth*, **10**, 741–763, https://doi.org/10.5194/se-10-741-2019

De Filippis, L., Soligo, M. *et al.* 2012. Growth of fissure ridge travertines from geothermal springs of Denizli Basin, western Turkey. *Geological Society of America Bulletin*, **124**, 1629–1645, https://doi.org/10.1130/B30606.1

Delvaux, D. and Sperner, B. 2003. New aspects of tectonic stress inversion with reference to the TENSOR Program.*Geological Society, London, Special Publications*, **212**, 75–100, https://doi.org/10.1144/GSL.SP.2003.212.01.06

Delvaux, D., Moeys, R., Stapel, G., Melnikov, A. and Ermikov, V. 1995. Palaeostress reconstructions and geodynamics of the Baikal region, Central Asia, Part I. Palaeozoic and Mesozoic pre-rift evolution. *Tectonophysics*, **252**, 61–101, https://doi.org/10.1016/0040-1951(95)00090-9

Dubois, C., Quinif, Y. *et al.* 2014. The process of ghost-rock karstification and its role in the formation of cave systems. *Earth Science Reviews*, **131**, 116–148, https://doi.org/10.1016/j.earscirev.2014.01.006

Ferrill, D.A. and Morris, A.P. 2003. Dilational normal faults. *Journal of Structural Geology*, **25**, 183–196, https://doi.org/10.1016/S0191-8141(02)00029-9

Frenzel, M. and Woodcock, N.H. 2014. Cockade breccia: product of mineralisation along dilational faults. *Journal of Structural Geology*, **68**, 194–206, https://doi.org/10.1016/j.jsg.2014.09.001

García Carmona, J., Gómez Morales, J. and Rodríguez Clemente, R. 2003. Rhombohedral-scalenohedral calcite transition produced by adjusting the solution electrical conductivity in the system $Ca(OH)_2$-CO_2-H_2O. *Journal of Colloid and Interface Science*, **261**, 434–440, https://doi.org/10.1016/S0021-9797(03)00149-8

George Anniss, L. and Smith, S. 1927. The geology of the Saltern Cove area, Torbay. *Quarterly Journal of the Geological Society, London*, **83**, 492–500, https://doi.org/10.1144/GSL.JGS.1927.083.01-05.19

Gill, W. and Kuenen, P. 1957. Sand volcanoes on slumps in the carboniferous of County Clare, Ireland. *Quarterly Journal of the Geological Society, London*, **CXIII**, 441–460, https://doi.org/10.1144/GSL.JGS.1957.113.01-04.19

Guoyi, D., Morrison, G. and Jaireth, S. 1995. Quartz textures in epithermal veins, Queensland – classification, origin, and implication. *Economic Geology*, **90**, 1841–1856, https://doi.org/10.2113/gsecongeo.90.6.1841

Harvey, M.J., Stewart, S.A., Wilkinson, J.J., Ruffell, A.H. and Shail, R.K. 1994. Tectonic evolution of the Plymouth Bay Basin. *Geoscience in South-West England*, **8**, 271–278.

Hauselmann, P., Jeannin, P.-Y. and Bitterli, T. 1999. Relationships between karst and tectonics: case-study of the cave system north of Lake Thun (Bern, Switzerland). *Geodinamica Acta*, **12**, 377–388.

Healy, D., Rizzo, R.E. *et al.* 2017. *FracPaQ: a MATLAB™ Toolbox for the Quantification of Fracture Patterns*, https://doi.org/10.1016/j.jsg.2016.12.003

Henson, M.R. 1971. *The Permo-Triassic Rocks of South Devon*. University of Exeter.

Holdsworth, R.E., McCaffrey, K.J.W. *et al.* 2019. Natural fracture propping and earthquake-induced oil migration in fractured basement reservoirs. *Geology*, **47**, 700–704, https://doi.org/10.1130/G46280.1

Holdsworth, R.E., Trice, R. *et al.* 2020. The nature and age of basement host rocks and fissure fills in the Lancaster field fractured reservoir, west of Shetland. *Journal of the Geological Society, London*, https://doi.org/10.1144/jgs2019-142

Holloway, S. and Chadwick, R.A. 1986. The Sticklepath–Lustleigh fault zone: Tertiary sinistral reactivation of a Variscan dextral strike-slip fault. *Journal of the Geological Society, London*, **143**, 447–452, https://doi.org/10.1144/gsjgs.143.3.0447

Hurst, A., Scott, A. and Vigorito, M. 2011. Physical characteristics of sand injectites. *Earth-Science Reviews*, **106**, 215–246, https://doi.org/10.1016/j.earscirev.2011.02.004

Kettermann, M., Von Hagke, C., Van Gent, H.W., Grützner, C. and Urai, J.L. 2016. Dilatant normal faulting in jointed cohesive rocks: a physical model study. *Solid Earth*, **7**, 843–856, https://doi.org/10.5194/se-7-843-2016

Kettermann, M., Weismuller, C., voc Hagke, C., Reicherter, K. and Urai, J.L. 2019. Large near-surface block rotations at normal faults of the Iceland rift: evolution of tectonic caves and dilatancy. *Geology*, **47**, 781–785, https://doi.org/10.1130/G46158.1

Leveridge, B.E. and Hartley, A.J. 2003. The Variscan Orogeny: Devonian/Carboniferous basins in SW England and South Wales. *In*: Brenchley, P.J. & Rawson, P.F. (eds) *The Geology of England and Wales.* Geological Society, London, 225–255.

Lundberg, J. and McFarlane, D. 2007. Pleistocene depositional history in a periglacial terrane: a 500 k.y. record from Kent's Cavern, Devon, United Kingdom. *Geosphere*, **3**, 199–219, https://doi.org/10.1130/GES00085.1

Martill, D.M. and Hudson, J.D. 1989. Injection clastic dykes in the Lower Oxford Clay (Jurassic) of central England: relationship to compaction and concretion formation. *Sedimentology*, **36**, 1127–1133, https://doi.org/10.1111/j.1365-3091.1989.tb01546.x

Milodowski, A.E., Bath, A. and Norris, S. 2018. Palaeohydrogeology using geochemical, isotopic and mineralogical analyses: salinity and redox evolution in a deep groundwater system through Quaternary glacial cycles. *Applied Geochemistry*, **97**, 40–60, https://doi.org/10.1016/j.apgeochem.2018.07.008

Muir-Wood, R. and King, G.C.P. 1993. Hydrological signatures of earthquake strain. *Journal of Geophysical Research: Solid Earth*, **98**, 22035–22068, https://doi.org/10.1029/93JB02219

Narayan, N., Gluyas, J. and Adams, C. 2018. Is the UK in hot water? *Geoscientist*, **28**, 10–15, https://doi.org/10.1144/geosci2018-014

Ortega, O.J., Marrett, R.A. and Laubach, S.E. 2006. A scale-independent approach to fracture intensity and average spacing measurement. *American Association of Petroleum Geologists Bulletin*, **90**, 193–208, https://doi.org/10.1306/08250505059

Paquette, J., Ward, W.B. and Reeder, R.J. 1993. Compositional Zoning and Crystal Growth Mechanisms in Carbonates: a New Look at Microfabrics Imaged by Cathodoluminescence Microscopy. *In*: Rezak, R. & Lavoie, D.L. (eds) *Carbonate Microfabrics*. Springer, New York, 243–252, https://doi.org/10.1007/978-1-4684-9421-1_18

Peterson, G.L. 1967. Flow structures in sandstone dikes. *Sedimentary Geology*, **2**, 177–190, https://doi.org/10.1016/0037-0738(68)90024-9

Petit, J.P. 1987. Criteria for the sense of movement on fault surfaces in brittle rocks. *Journal of Structural Geology*, **9**, 597–608, https://doi.org/10.1016/0191-8141(87)90145-3

Popov, P., Qin, G., Bi, L., Efendiev, Y., Ewing, R. and Li, J. 2009. Multiphysics and multiscale methods for modeling fluid flow through naturally fractured carbonate karst reservoirs. *SPE Reservoir Evaluation & Engineering*, **12**, 218–231, https://doi.org/10.2118/105378-PA

Ramsay, J.G. 1980. The crack-seal mechanism of rock deformation. *Nature*, **284**, 135–139, https://doi.org/10.1038/284135a0

Richter, D. 1966. On the New Red Sandstone Neptunian dykes of the Tor Bay area (Devonshire). *Proceedings of the Geologists' Association*, **77**, 173-IN3, https://doi.org/10.1016/S0016-7878(66)80068-8

Rowe, C. 2013. Shaking loose: sand volcanoes and Jurassic earthquakes. *Geology*, **41**, 1135–1136, https://doi.org/10.1130/focus102013.1

Rowland, J., Baker, E. *et al.* 2007. Fault growth at a nascent slow-spreading ridge: 2005 Dabbahu rifting episode, Afar. *Geophysics Journal International*, **171**, 1226–1246, https://doi.org/10.1111/j.1365-246X.2007.03584.x

Ruffell, A.H. and Shelton, R.G. 2000. Permian to Late Triassic post-orogenic collapse and early Atlantic rifting, deserts, evaporating seas and mass extinctions. *In*: Woodcock, N. and Strachan, R. (eds) *Geological History of Britain and Ireland*. Blackwell Science, Oxford, 297–313.

Russell, A. 1929. On the occurrence of native gold at Hope's Nose, Torquay, Devonshire. *Mineralogical Magazine and Journal of the Mineralogical Society*, **22**, 159–162, https://doi.org/10.1180/minmag.1929.022.126.04

Sanderson, D.J. and Nixon, C.W. 2015. The use of topology in fracture network characterization. *Journal of Structural Geology*, **72**, 55–66, https://doi.org/10.1016/j.jsg.2015.01.005

Schlische, R.W. and Ackermann, R.V. 1995. Kinematic significance of sediment-filled fissures in the North Mountain Basalt, Fundy rift basin, Nova Scotia, Canada. *Journal of Structural Geology*, **17**, 987–996, https://doi.org/10.1016/0191-8141(94)00114-F

Scrivener, R.C., Darbyshire, D.P.F. and Shepherd, T.J. 1994. Timing and significance of cross course mineralization in SW England. *Journal of the Geological Society, London*, **151**, 587–590, https://doi.org/10.1144/gsjgs.151.4.0587

Shail, R.K. and Leveridge, B.E. 2009. The Rhenohercynian passive margin of SW England: development, inversion and extensional reactivation. *Comptes Rendus – Geoscience*, **341**, 140–155, https://doi.org/10.1016/j.crte.2008.11.002

Shail, R.K. and Wilkinson, J.J. 1994. Late- to post-Variscan extensional tectonics in south Cornwall. *Proceedings of the Ussher Society*, **8**, 262–270.

Shannon, W.G. 1928. The geology of the Torquay district. *Proceedings of the Geologists' Association*, **39**, 103-136,https://doi.org/10.1016/S0016-7878(28)80020-4

Shepard, T.J., Bouch, J.E. *et al.* 2005. Permo-Triassic unconformity-related Au–Pd mineralisation, South Devon, UK: new insights and the European perspective. *Mineralium Deposita*, **40**, 24–44, https://doi.org/10.1007/s00126-004-0459-3

Sibson, R.H. 1981. Fluid flow accompanying faulting: field evidence and models. *Earthquake Prediction*, **4**, 593–603, https://doi.org/10.1029/ME004p0593

Sibson, R.H. 1990. Conditions for fault-valve behaviour. *Geological Society, London*, Special Publications, **54**, 15–28, https://doi.org/10.1144/GSL.SP.1990.054.01.02

Sibson, R.H. 1994. Crustal stress, faulting and fluid flow. Geological Society, London, Special Publications, **78**, 69–84, https://doi.org/10.1144/GSL.SP.1994.078.01.07

Sibson, R.H. 1996. Structural permeability of fluid-driven fault-fracture meshes. *Journal of Structural Geology*, **18**, 1031–1042, https://doi.org/10.1016/0191-8141(96)00032-6

Sibson, R.H., Moore, J.M.M. and Rankin, A.H. 1975. Seismic pumping –a hydrothermal fluid transport mechanism. *Journal of the Geological Society, London*, **131**, 653–659, https://doi.org/10.1144/gsjgs.131.6.0653

Siddoway, C.S. and Gehrels, G.E. 2014. Basement-hosted sandstone injectites of Colorado: a vestige of the Neoproterozoic revealed through detrital zircon provenance analysis. *Lithosphere*, **6**, 403–408, https://doi.org/10.1130/L390.1

Siddoway, C.S., Palladino, G., Prosser, G., Freedman, D. and Duckworth, W.C. 2019. Basement-hosted sand injectites: use of field examples to advance understanding of hydrocarbon reservoirs in fractured crystalline basement rocks. *Geological Society, London, Special Publications*, **493**, https://doi.org/10.1144/SP493-2018-140

Smart, P.L., Palmer, R.J., Whitaker, F. and Paul Wright, V. 1988. Neptunian dikes and fissure fills. *In*: James, N.P. and Choquette, P.W. (eds) *Paleokarst*. Springer, New York, 149–150.

Smith, K.G. 1952. Structure plan of clastic dikes. *Eos, Transactions American Geophysical Union*, **33**, 889–892, https://doi.org/10.1029/TR033i006p00889

Strange, P.J. 2001. Torquay 1:50 000 Geology Series Map. NERC,Swindon.

Thomas, H.H. 1909. A contribution to the petrography of the New Red Sandstone in the West of England. *Quarterly Journal of the Geological Society*, **65**, 229–244, https://doi.org/10.1144/GSL.JGS.1909.065.01-04.18

Underhill, J.R. and Stoneley, R. 1998. Introduction to the development, evolution and petroleum geology of the Wessex Basin. *Geological Society, London, Special Publications*, **133**, 1–18, https://doi.org/10.1144/GSL.SP.1998.133.01.01

Ussher, W.A.E. 1903. The geology of the country around Torquay: explanation of sheet 350. *Memoirs of the Geological Survey of Great Britain, England and Wales*. HMSO, London.

van Gent, H.W., Holland, M., Urai, J.L. and Loosveld, R. 2010. Evolution of fault zones in carbonates with mechanical stratigraphy - Insights from scale models using layered cohesive powder. *Journal of Structural Geology*, **32**, 1375–1391, https://doi.org/10.1016/j.jsg.2009.05.006

von Hagke, C., Kettermann, M., Bitsch, N., Bücken, D., Weismüller, C. and Urai, J.L. 2019. The effect of obliquity of slip in normal faults on distribution of open fractures. *Frontiers in Earth Science*, **7**, 18, https://doi.org/10.3389/feart.2019.00018

Walker, R.J., Holdsworth, R.E., Imber, J. and Ellis, D. 2011. The development of cavities and clastic infills along fault-related fractures in Tertiary basalts on the NE Atlantic margin. *Journal of Structural Geology*, **33**, 92–106, https://doi.org/10.1016/j.jsg.2010.12.001

Walker, R.J., Holdsworth, R.E., Imber, J., Faulkner, D.R. and Armitage, P.J. 2013. Fault zone architecture and fluid flow in interlayered basaltic volcaniclastic–crystalline sequences. *Journal of Structural Geology*, **51**, 92–104, https://doi.org/10.1016/j.jsg.2013.03.004

Wall, G.R.T. and Jenkyns, H.C. 2004. The age, origin and tectonic significance of Mesozoic sediment-filled fissures in the Mendip Hills (SW England): implications for extension models and Jurassic sea-level curves. *Geological Magazine*, **141**, 471–504, https://doi.org/10.1017/S0016756804009185

Wallace, R.E. 1951. Geometry of shearing stress and relation to faulting. *The Journal of Geology*, **59**, 118–130, https://doi.org/10.1086/625831

Walton, M.S.J. and O'Sullivan, R.B. 1950. The intrusive mechanics of a clastic dike. *American Journal of Science*, **248**, 1–21, https://doi.org/10.2475/ajs.248.1.1

Williams, G.D. 1986. The Bristol–Mendip foreland thrust belt. *Journal of the Geological Society, London*, **143**, 63–73, https://doi.org/10.1144/gsjgs.143.1.0063

Woodcock, N.H., Miller, A.V.M. and Woodhouse, C.D. 2014. Chaotic breccia zones on the Pembroke Peninsula, south Wales: evidence for collapse into voids along dilational faults. *Journal of Structural Geology*, **69**, 91e107, https://doi.org/10.1016/j.jsg.2014.09.019

Wright, V., Woodcock, N.H. and Dickson, J.A.D. 2009. Fissure fills along faults: Variscan examples from Gower, South Wales. *Geological Magazine*, **146**, 890–902, https://doi.org/10.1017/S001675680999001X

Yang, H., Zhu, G., Wang, Y., Su, J. and Zhang, B. 2014. The geological characteristics of reservoirs and major controlling factors of hydrocarbon accumulation in the Ordovician of Tazhong area, Tarim Basin. *Energy Exploration and Exploitation*, **32**, 345–368.